

Metallophthalocyanines derived with phenyl sulfide by bridging triazole using click chemistry: Synthesis, Computational Study, Redox Chemistry and Catalytic Activity



Hüseyin Karaca^{a,*}, Nagihan Çaylak Delibaş^b, Serap Sağlam^a, Hasan Pişkin^c, Serdar Sezer^d, Tuncer Hökelek^e, Murat Teker^a

^a Department of Chemistry, Sakarya University, 54187 Sakarya, Turkey

^b Department of Physics, Sakarya University, 54187, Esentepe, Sakarya, Turkey

^c Boğaziçi University, Department of Physics, 34342, Bebek, İstanbul, Turkey

^d Department of Pharmacology, Faculty of Medicine, Suleyman Demirel University, Isparta, Turkey

^e Department of Physics, Hacettepe University, 06800 Beytepe-Ankara, Turkey

ARTICLE INFO

Article history:

Received 23 August 2020

Revised 3 February 2021

Accepted 26 February 2021

Available online 23 March 2021

Keywords:

Phthalocyanine
triazole
computational
redox
catalysis
click

ABSTRACT

Synthesis and characterization of new metallophthalocyanines ($M = \text{Zn, Co (II) and Ni (II)}$) carrying four new triazole units in peripheral positions was presented in this paper. First, 4-(prop-2-yn-1-yloxy)phthalonitrile, **3**, was synthesized. Second, azidomethyl phenyl sulfide, **4**, was added to this structure in order to obtain a triazole unit catalyzed by sodium ascorbate and $\text{CuSO}_4 \cdot 5\text{H}_2\text{O}$ in DMSO. Common spectroscopic methods such as FT-IR, $^1\text{H-NMR}$, $^{13}\text{C-NMR}$, HRMS and UV-Vis spectroscopy techniques were used for characterization of synthesized structures. The molecular structure of the phthalonitrile compound **5** was confirmed by single-crystal X-ray diffraction experiment. Moreover, by using HF and B3LYP method and 6-31++g(d,p) basis set, ^1H and ^{13}C NMR chemical shifts, IR and UV-vis spectrums were theoretically calculated in gas phase for the optimized structure of **5**. The obtained FTIR spectra and NMR spectra showed that the desired molecules were synthesized, and mass spectra confirmed these molecules. Electronic absorption spectra have shown that phthalocyanines are non-aggregable molecules. The cyclic voltammetry data of the phthalocyanines has shown that the **Pc-6** has two reduction reactions and two oxidation reactions while the **Pc-7** and **Pc-8** have one reduction reaction and one oxidation reaction. Furthermore, the cobalt(II)phthalocyanine, **Pc-7**, was investigated as oxidation catalyst for the catalytic oxidation of 2-mercaptoethanol. Turnover number, initial reaction rate and the oxygen consumption values were found in the catalytic oxidation of 2-mercaptoethanol as 18.09, 0.12 $\mu\text{mol.s}^{-1}$ and 6.88 $\mu\text{mol.min}^{-1}$, respectively.

© 2021 Elsevier B.V. All rights reserved.

1. Introduction

Phthalocyanine is one of the tetraizoindole derivative, which is one of the main topics of interest in both basic science and applied studies last three decades. Over the years, it has become the subject of more research [1-8]. Derivatization of phthalocyanines with various functional groups, either peripheral or non-peripheral, yields unique properties. Studies on the potential uses of these unique properties of phthalocyanines on the remarkable areas such as dyes and catalysts [9-13], sensitive elements in chemical sensors [14-18], organic photovoltaic devices [19-24], electrochromic display devices [25-31], photodynamic therapy of cancer and other

medical applications [32-43], fuel cell applications [44-54], electrocatalysis [55-66], photovoltaic cell elements in energy production [67-81], molecular metals and conductive polymers [82-87]. It is important not only to improve the derivatization properties of phthalocyanines, but also to make them usable. Because only the phthalocyanine macro ring is not soluble. Derivation is essential to be soluble in both water and organic solvents [88-90].

Recently, triazoles have received increasing attention as an important class of heterocyclic compounds in medicinal chemistry and other chemistry applications [91-98]. In chemical synthesis, "click" chemistry is a class of biocompatible small molecule reactions that are commonly used in bioconjugation, which allow combining preferred substrates with specific biomolecules. It is also seen that click chemistry has begun to be applied in phthalocyanines [99-101]. It was thought that the triazole unit would add IR

* Corresponding author.

E-mail address: [karaca@sakarya.edu.tr](mailto:karakac@sakarya.edu.tr) (H. Karaca).

property close to phthalocyanine. The absorbance of the obtained zinc phthalocyanine at 708 nm in the UV-visible spectrum supported this idea.

In this study, 4-((3-((phenylthio)methyl)-3H-1,2,4-triazol-5-yl)methoxy)phthalonitrile, **5**, as monomer and metallophthalocyanines were synthesized. The molecular structure of compound **5** was confirmed by the single crystal X-ray diffraction (XRD) method. The possible intermolecular interactions present within the single crystal of **5** have been revealed by the analysis of XRD data. Furthermore, the structural and spectral properties of compounds **5** was computationally determined. We have investigated redox chemistry of triazole bridged phenyl sulfide-derived metallophthalocyanines. The catalytic activity of Co (II) phthalocyanine was investigated. This is based on the oxidation reaction of 2-mercaptoethanol with dissolved oxygen. The novel designed and synthesized metallophthalocyanines having triazole bridged phenyl sulfide on the periphery were characterized by ¹H-NMR, ¹³C-NMR, IR, MALDI-TOF, and UV/Vis spectra and then reported.

2. Experimental

2.1. General

The glassware was heated in an oven at 150°C for 1 hour and then cooled under a nitrogen atmosphere and used in the experiments. The reaction solvents were distilled off with the indicated drying agents: DMAE (CaH₂), DMF (CaH₂). All chemicals were purchased from commercial suppliers and used directly. Barnstead Electrothermal 9200 model melting point device were used to determine melting points of synthesized molecules. Merck Silica Gel 60 was used for flash column chromatography in a thick-walled glass column. Thin layer chromatography (TLC) was used to enable monitoring of the reaction through by using the silica gel precoated aluminum sheet (Merck Silica Gel PF-254). Polymolybdenum phosphoric acid solution in ethanol and UV light were used to visualize stains on the TLC plate. Solvents was evaporated under vacuum by using a rotary evaporator after the All extracts were dried over anhydrous magnesium sulfate.

2.2. Spectroscopy

¹H NMR and ¹³C NMR spectra were recorded in CDCl₃ and DMSO-d₆ using a VARIAN Infinity Plus 300 MHz NMR spectrometer. The ppm was used to express chemical shifts relative to CDCl₃ (δ7.26 and 77.0 for ¹H and ¹³C NMR, respectively) and TMS as the internal standard. FT-IR spectra were recorded on a Perkin Elmer Spectrum Two FT-IR spectrometer. HRMS and MALDI-TOF spectra were recorded on an Agilent Technologies 6530 Accurate-Mass Q-TOF LC/MS device. UV-visible spectrums were recorded on a Shimadzu UV 2600 model Spectrophotometer.

2.3. Catalytic oxidation of 2-mercaptoethanol

CyberScan DO 300 oxygen meter was used to measure the dissolved oxygen in reaction mixture in the closed system. Co(II)phthalocyanine (Co(II)Pc) (**Pc-7**) was dissolved as 0.380 μmol in 50 mL THF. The reaction vessel was bubbled with air bubbles to saturate the solution to oxygen. We have used air oxygen for this oxidation. Then 2.07 mmol 2-mercaptoethanol was added. A 5500:1 ratio of 2-mercaptoethanol and Co (II) phthalocyanine, which is a good ratio of catalytic activity, was used. After adding the 2-mercaptoethanol, 1 mL of 0.25 wt% aqueous sodium hydroxide solution was poured into the reaction vessel and system was closed. Measurement of the dissolved oxygen remaining in the reaction mixture from the oxidation reaction was

started simultaneously and then time dependent oxygen consumption was calculated. The characterization of the catalytic activity of Co(II)phthalocyanine **Pc-7** was set by turnover number, TON (conversion mol oxygen per mol phthalocyanine), initial reaction rate (μmol oxygen consumption per second) and the oxygen consumption (μmol/min) [102-105].

The calculation of the turnover number is made by dividing moles of oxygen by moles of phthalocyanine. The initial rate of the reaction is calculated by setting the first order derivative of the reaction rate equation to zero. The oxygen consumption is calculated by dividing moles of oxygen by time.

2.4. Synthesis

2.4.1. 4-(prop-2-yn-1-yloxy)phthalonitrile, **3**

1.00 g (5.78 mmol) 4-nitrophthalonitril and 6.00 g (43.46 mmol) K₂CO₃ were stirred in 12 mL DMSO in a half hour. Then 0.32 g (5.78 mmol) propargyl alcohol was added and continued stirring for next three hours under the argon atmosphere at room temperature. 100 mL water was poured into the reaction vessel, then the crude product was extracted with DCM. The eluent containing the product was dried over MgSO₄, then the solvent was dried on a rotary evaporator under vacuum. The obtained product to afford **3** as solid was cleaned by column chromatography on silica gel by using the ethyl acetate/hexane as eluent. Green solid (53.70 mg, 81% chemical yield). Melting point: 108 °C. FT-IR (ATR System, cm⁻¹): 3287, 3119, 3077, 2230, 2135, 1596, 1494, 1321, 1260. ¹H NMR (300 MHz, CDCl₃) δ: δ 8.09 (d, J = 8.8 Hz, 1H), 7.80 (d, J = 2.5 Hz, 1H), 7.49 (dd, J = 8.8, 2.7 Hz, 1H), 5.00 (s, 2H), 3.71 (d, J = 1.6 Hz, 1H). ¹³C NMR (75 MHz, CDCl₃) δ: 160.5, 135.2, 120.2, 119.9, 117.4, 115.5, 115.2, 108.2, 77.8, 76.2, 56.6. Anal. Calc. for C, 72.52; H, 3.32; N, 15.38 %. Found: C:72.02; H:3.42; N:15.48 %. HRMS: m/z [M] calcd.182.18 For C₁₃H₁₁NO: found [M+H]⁺ 199.15.

2.4.2. 4-((3-((phenylthio)methyl)-3H-1,2,4-triazol-5-yl)methoxy)phthalonitrile, **5**

0.86 g (4.70 mmol) **3** and 0.70 g (4.70 mmol) azidomethyl phenyl sulfide **4** were dissolved in 18 mL DMSO in a round-bottom flask and stirred under the nitrogen atmosphere for half an hour. Then 0.13 g (0.47 mmol) sodium ascorbate and 0.12 g (0.47 mmol) CuSO₄.5H₂O were added together into the flask and continued stirring for 24 hours at room temperature under the nitrogen atmosphere. 200 mL water was added into the reaction mixture. The white precipitate was extracted with DCM. The DCM containing the product was dried over MgSO₄, then the solvent was dried on a rotary evaporator under vacuum. The obtained was cleaned by column chromatography on silica gel by using the ethyl acetate/hexane as eluent. The white solid (1.47 g, 89.96 % chemical yield). Melting point: between 180, 190 °C. FT-IR (ATR System, cm⁻¹): 3185, 3125, 3085, 2991, 2941, 2230, 1592, 1500, 1471, 1318, 1252, 1224, 1058, 987, 852, 809, 746, 690, 521, 490. ¹H NMR (300 MHz, CDCl₃) δ 7.71 (d, J = 8.3 Hz, 1H), 7.60 (s, 1H), 7.33 (d, J = 2.4 Hz, 1H), 7.24 (s, 3H), 7.21–7.18 (m, 3H), 5.59 (s, 2H), 5.22 (s, 2H). ¹³C NMR (75 MHz, DMSO-d₆) δ 161.30, 135.53, 132.27, 131.68, 129.81, 129.10, 123.12, 123.09, 120.51, 119.72, 117.67, 115.76, 115.34, 108.10, 62.69, 54.28. Anal. Calc. For C:62.23; H:3.77; N:20.16; S:9.23 %. Found: C,61.82; H,3.65; N:20.36; S:9.32 %. HRMS: m/z [M] calcd. 347.40 For C₂₁H₁₃N₃O: found [M+H]⁺ 348.25.

2.4.3. General procedure for the synthesis of phthalocyanines, **Pc-6**, **Pc-7** and **Pc-8**

Metal salts, Zn(OAc)₂.2H₂O, Co(Oac)₂.4H₂O and NiCl₂.2H₂O, were taken at 1/4 ratio relative to the phthalonitrile, **5**, to synthesize the metallophthalocyanines. Phthalonitrile, **5**, was dissolved in a mixture of DMEA/DMF (1:2). The mixture was stirred for half

an hour, metal salt was added to the mixture and continued stirring at 150 °C for 24 hours under the nitrogen atmosphere. Reaction was finished after TLC controlling. Then the reaction mixture was poured into the mixture of methanol water (1:1) to stop the reaction. Obtained dark green solid was dried under vacuum and columned by hexane: ethyl acetate.

2.4.4. Zinc phthalocyanine, **Pc-6**

Dark green solid, mp >300 °C, (147 mg, 40.1 % chemical yield). FT-IR (ATR System, cm⁻¹): 3054, 2919, 2851, 1608, 1474, 1411, 1343, 1224, 1046, 815, 746, 690, 456. ¹H NMR (300 MHz, DMSO-d₆) δ 8.54–8.36 (m, 8H), 7.93–7.79 (m, 8H), 7.53–7.39 (m, 8H), 7.38–7.21 (m, 12H), 6.13–5.97 (m, 8H), 5.79–5.68 (m, 8H). Anal. Calc. for C, 59.44; H, 3.60; N, 19.25; O, 4.40; S, 8.81; Zn, 4.49 %. Found: C, 59.32; H, 3.69; N, 19.19 %. MALDI-TOF MS: m/z [M]⁺ calcd. For C₇₂H₅₂N₂₀O₄S₄Zn: 1454.96; found [M+Na]⁺ 1477.65.

2.4.5. Cobalt (II) phthalocyanine, **Pc-7**

Dark green solid, mp >300 °C, (75mg, 30.8 % chemical yield). FT-IR (ATR System, cm⁻¹): 3138, 3057, 2919, 2851, 1602, 1477, 1408, 1327, 1277, 1227, 1096, 1046, 821, 743, 690, 487. Anal. Calc. For C, 59.70; H, 3.62; N, 19.34; O, 4.42; S, 8.85; Co, 4.07 %. Found: C, 59.64; H, 3.75; N, 19.21; S, 8.73 %. MALDI-TOF MS: m/z [M]⁺ calcd. For C₇₂H₅₂N₂₀O₄S₄Co: 1448.52; found [M+4H]⁺: 1452.36.

2.4.6. Nickel (II) phthalocyanine, **Pc-8**

Dark green solid, mp >300 °C, (130 mg, 53.5 % chemical yield). FT-IR (ATR System, cm⁻¹): 2922, 2854, 1605, 1471, 1346, 1230, 1093, 1043, 812, 743, 690. ¹H NMR (300 MHz, DMSO-d₆) δ 8.34–8.06 (m, 8H), 7.51–7.09 (m, 28H), 6.05–5.78 (m, 8H), 5.35–5.17 (m, 8H). Anal. Calc. For C₇₂H₅₂N₂₀O₄S₄Ni C, 59.71; H, 3.62; N, 19.34; Ni, 4.05; O, 4.42; S, 8.85 %. Found: C, 59.62; H, 3.68; N, 19.25; S 8.74 %. MALDI-TOF MS: m/z [M]⁺ calcd. For C₇₂H₅₂N₂₀O₄S₄Ni: 1448.28; found [M+K]⁺: 1452.28.

2.5. X-ray data collection and refinement for the compound 5

Bruker APEX II Quazar three circle diffractometer with monochromated Mo-K α radiation ($\lambda=0.71073 \text{ \AA}$) was used to collect the HKL data of the solid-stated single crystal of **5**. For the experiment, a block-like colourless crystal was taken by dimensions of $0.18 \times 0.12 \times 0.09$ (mm). Totally, 25761 reflections were observed, 7481 reflections were independent, and 7205 reflections were greater than $2\sigma(F^2)$. The crystal structure was solved by using the direct methods in SHELXS and refined by the least-squares (F²) method provided by SHELXL in Olex2 software. Firstly, all of the atoms (except hydrogens) were placed correctly as isotropic. Then, refined as anisotropic. All the hydrogen atoms were placed geometrically, and the complete structure was refined a few times to get best fit. For the resulted "cif" file, a twinning was observed with the FCF based twin law (0 0 1) [2 0 5] (BASF 0.14). Therefore, a new HKLF 5 file was generated by using "TwinRotMat" function given in PLATON software and the resulted structure was refined a few more times. Finally, the goodness of fit (S) has been obtained as 1.08. Table 1 presents the summary of crystallographic information, data collection and the refinement parameters. In addition, the solid-stated crystal stabilization dynamics have been analysed by the PLATON program [106]. The check cif validation done at the check-CIF/PLATON web-based IUCr service [107]. The crystallographic information file (cif) has been uploaded to the data centre with CCDC number 2021080.

Data collection: Bruker Instrument Service [108]; **data integration and reduction:** SAINT V8.34A [109]; **absorption correction:** multi-scan method implemented in SADABS [110]; **program(s) used to solve structure:** SHELXS; **program(s) used to refine structure:** SHELXL [111]; **molecular graphics and software used to prepare material for publication:** Olex2 [112].

Table 1

Crystallographic information, data collection and refinement parameters for monomer phthalonitrile **5**.

CCDC Number	2021080
Empirical formula	C ₁₈ H ₁₃ N ₅ OS
Formula weight (g/mol)	347.39
Temperature (K)	100
Wavelength (Å)	Mo K α radiation (0.71073)
Crystal system	Monoclinic
Space group	Pc
a (Å)	11.7491 (6)
b (Å)	5.4135 (3)
c (Å)	26.1548 (13)
α (°)	90.0
β (°)	99.719 (3)
γ (°)	90.0
Volume (Å ³)	1639.67 (15)
Z	4
Crystal size (mm)	0.18 × 0.12 × 0.09
Crystal description	Block, colourless
Calculated density (g cm ⁻³)	1.407
Absorption coefficient μ (mm ⁻¹)	0.21
F (000)	720
θ range for data collection (°)	2.6° to 27.5°
h, k, l	-15/15, -7/7, -34/34
Reflections collected	25761
Independent reflections	7481
Data/restraints/parameters	7205 / 2 / 452
Goodness of fit on F ²	1.08
Final R indices (Data; I > 2σ[I])	R ₁ = 0.0663, wR ₂ = 0.1613
Largest diff. Peak and hole (e Å ⁻³)	0.56 and -0.79 with 0.042 R.M.S.

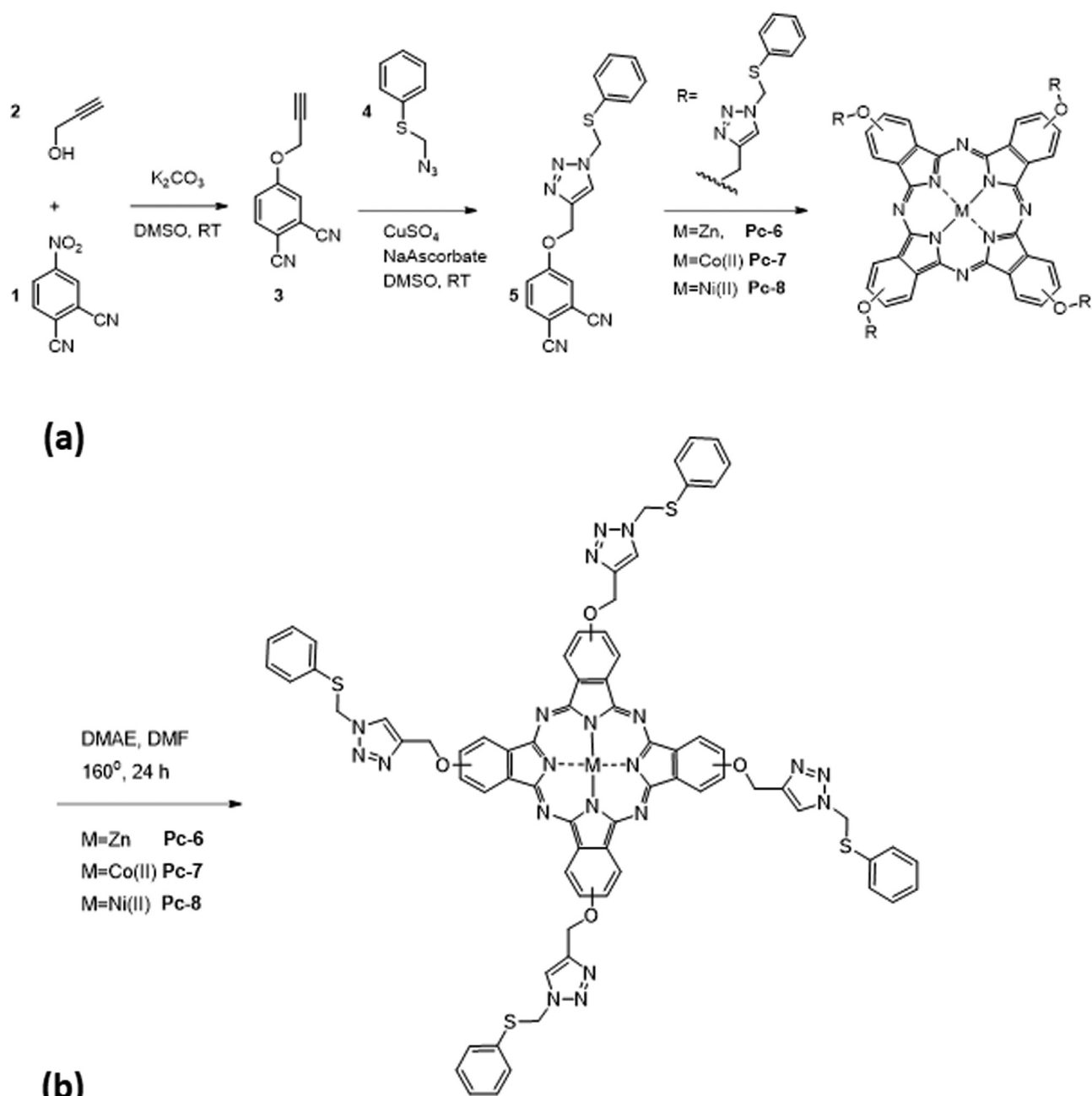
2.6. Quantum chemical calculation method

Quantum chemical calculations are realized in order to obtain HOMO, LUMO, ΔE , chemical hardness, global softness, electronegativity, nucleophilicity and chemical potential. A calculation of monomer phthalonitrile **5** was performed by using Gaussian 16W [113] and the resulted structure was visualized with the help of GausView 6.0.16 [114]. The quantum chemical calculations of monomer phthalonitrile **5** in gas phase were obtained by using of Hartree Fock and Becke-3-Parameter-Lee-Yang-Parr (B3LYP) [115] methods with 6-311++G(d,p) basis set.

3. Results and discussion

3.1. Synthesis

It is known from the literature that the binding of bulky substituents to phthalocyanines, either peripheral or non-peripheral positions, prevents aggregation, thereby increases the solubility of phthalocyanines in organic solvents and in aqueous media. In addition, the metal exchange at the center of the phthalocyanine affects the solubility of the phthalocyanines [1,2,88,89]. It was synthesized a triazole bridged phenyl sulfide at peripheral positions as phthalocyanine derivatizer. Thus, since a bulky group was formed, its solubility was expected to be high and so was it. The synthesis was started by the reaction of propargyl alcohol with 4-nitrophthalonitrile in the presence of potassium carbonate under nitrogen atmosphere and at room temperature. After the column chromatography isolation chemical yield was 81% and thus the compound **3** has been obtained via the SNAr type substitution reaction between propargyl alcohol **2** and 4-nitrophthalonitrile **1**. A triazole bridged phenyl sulfide-derived phthalonitrile **5** was synthesized by the catalytic reaction of compound **3** and azidomethyl phenyl sulfide with CuSO₄ and sodium ascorbate in DMSO at room temperature. The chemical yield was 89.96 % (Scheme 1(a)). We have previously published phthalocyanines having triazole functionality [99]. Moreover, these triazole bridged phenyl sulfide-



Scheme 1. (a) Synthesis of phthalonitrile 3, 5 and target phthalocyanine skeleton (b) Synthesis of target phthalocyanines **Pc-6**, **Pc-7** and **Pc-8**.

derived metallophthalocyanines are newly synthesized and investigated. This derivatization will provide phthalocyanines with new properties and application opportunities. In this study, the redox behavior of phthalocyanines together with the crystal structure of the **5** compounds were investigated. Such derivatization of Metallo Pcs will allow for increased solubility and biological activity [116]. We have reported the redox chemistry of these novel phthalocyanines.

The structures of compounds **3** and **5** are qualified by 1H and ^{13}C NMR spectra and approved by FT-IR spectra. The synthesized phthalonitrile **5** was used as initial monomer for synthesis of metallophthalocyanines **Pc-6**, **Pc-7** and **Pc-8**. $Zn(OAc)_2 \cdot 2H_2O$, $NiCl_2 \cdot 2H_2O$ and $Co(OAc)_2 \cdot 4H_2O$ salts have been used in cyclotrimerization of **5**, using DMAE as the catalyst at high temperature in DMF. An isomeric mixture of the desired metallo Pcs were synthesized as expected (Scheme 1 (b)). The 1H NMR spectra of

Pc-6 and **Pc-8** were received in DMSO. Moreover, elemental analysis and HRMS and MALDI-TOF measurements of synthesized compounds were taken. Thus, the structures of the synthesized MPCs were elucidated by 1H NMR technique. These structures were confirmed by FTIR spectra and molecular mass analysis.

3.2. Structure Elucidation

The FTIR spectra clearly shows that the desired compounds are synthesized successfully at each step of the synthesis. Fig. 1 shows calculated and experimental FTIR spectra. The band viewed at 1592 cm^{-1} in compound **5** can be attributed to C=C double bond. This band shifts to 1608 cm^{-1} in **Pc-6**, 1602 cm^{-1} in **Pc-7** and 1605 cm^{-1} in **Pc-8** because of extra aromatic rings and extra aromatization. The bands viewed at 2231 cm^{-1} in compound **3** and 2230 cm^{-1} in compound **5** can be attributed to C≡N triple nitrile bond

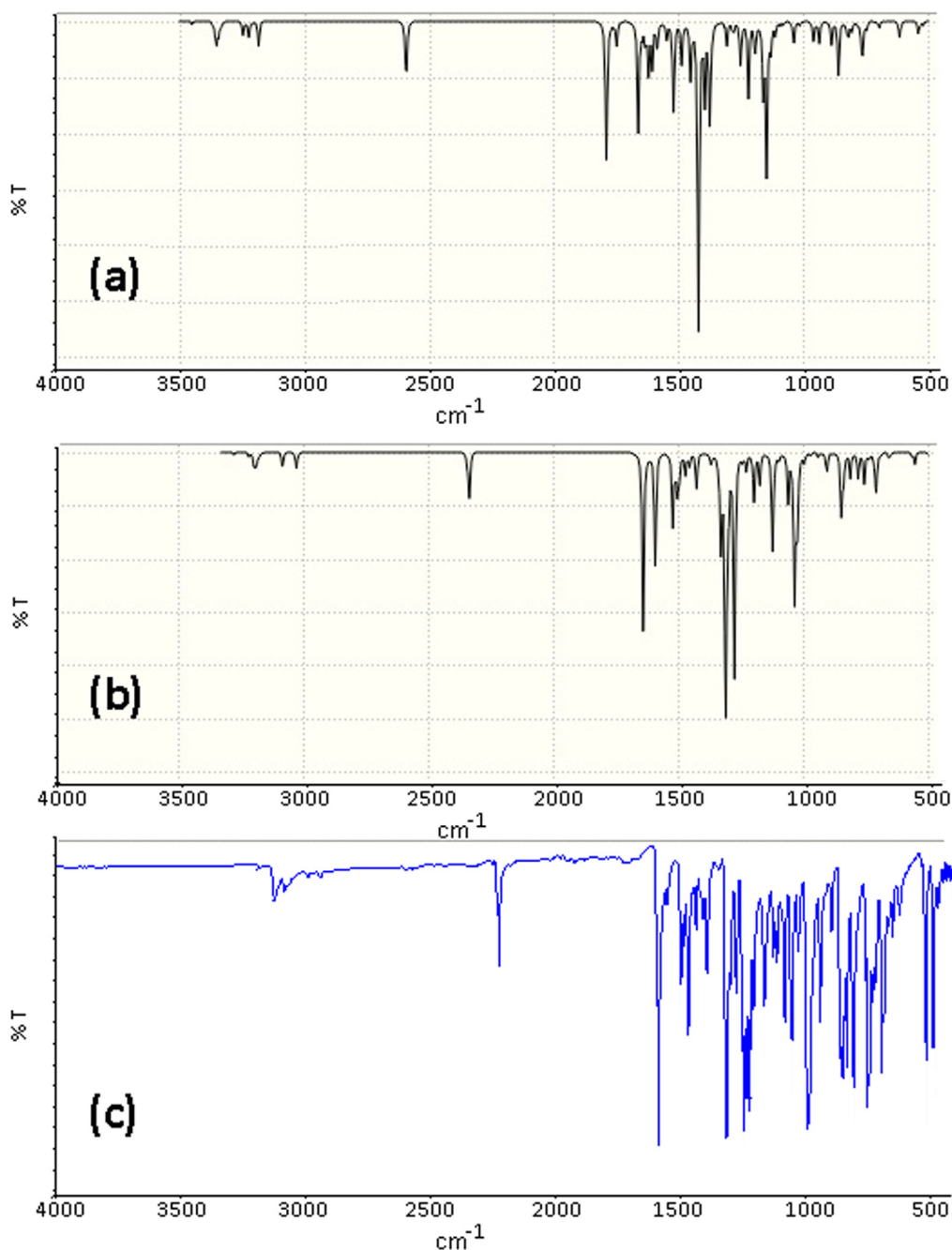


Fig. 1. The calculated (a) HF, (b) B3LYP and (c) experimental FTIR spectra.

stretching vibrations. Cyclotetramerization of monomer **5** and formation of phthalocyanines clearly show that this band at which is 2230 cm⁻¹ in the FTIR spectrum disappears. Other groups below 2000 cm⁻¹ do not have disturbing changes. The bands that is attributable to phthalocyanine skeletal vibrations [28,51] are seen at 3054, 2919, 2851, 1608, 1474, 1411, 1343, 1224, 1046, 815, 746, 690, 456 cm⁻¹ are observed for **Pc-6**. The phthalocyanines **Pc-7** and **Pc-8** show very similar peaks 3138-487 cm⁻¹ in Fig. 2.

The compounds **3** and **5** have mostly aromatic structure so most of the proton peaks are between 8-6 ppm. The compound **3** has an acetylenic hydrogen having a doublet peak at 3.71 ppm with J=1.6 Hz. This peak disappeared on the next step because of occurring the triazole unit by using acetylene. The compound **3** also have a second peak at 5.00 ppm under the aromatic region. The

compound **5** have four aliphatic protons as two CH₂ group. Both of the CH₂ groups have singlet proton NMR as expected, one is at 5.59 ppm and second is at 5.22 ppm. Fig. 3 shows calculated in HF and B3LYP and experimental NMR spectrums. The ¹H-NMR spectra of phthalocyanine of **Pc-6**, shows the peaks in aromatic region with small differences in chemical shifts. The peak of CH₂ groups are seen between 6.13-5.97 ppm for 8H and 5.79-5.68 ppm for 8H. These peaks of CH₂ groups **Pc-8** are seen between 6.05-5.78 for 8H and 5.35-5.17 ppm for 8H. These results are consistent. Since the paramagnetic nature of cobalt inhibited NMR recording, the ¹H-NMR spectrum of cobalt phthalocyanine, **Pc-7**, was not recorded.

The mass spectra of phthalocyanines, **Pc-6**, **Pc-7** and **Pc-8**, were also taken and shown in Fig. 4. Molecular ion peaks are identified 1477.65 as the [M+Na]⁺ for **Pc-6**, 1452.36 as the

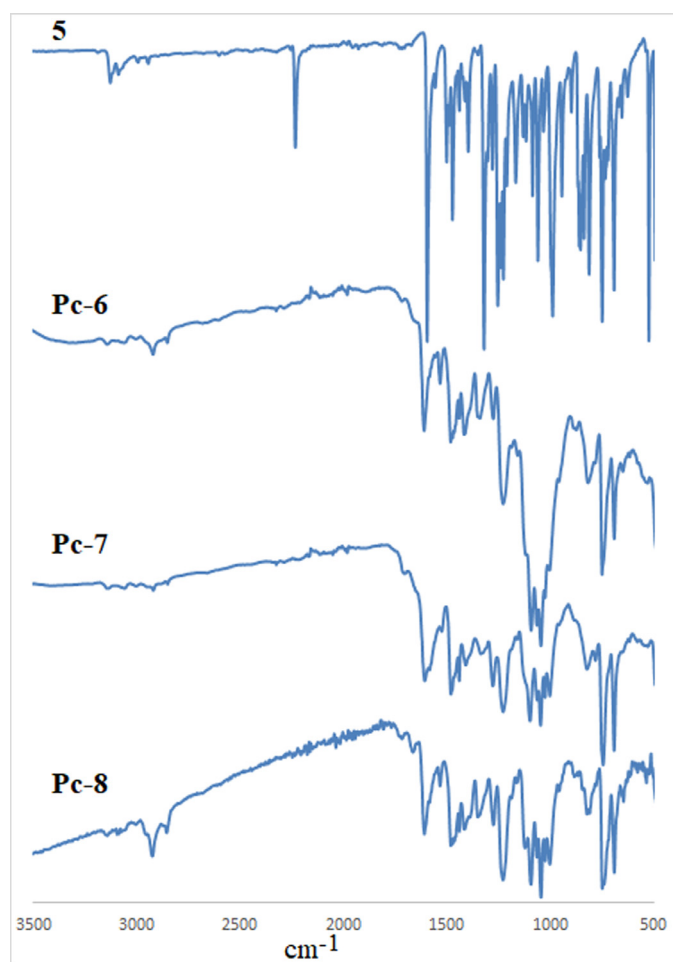


Fig. 2. FTIR spectra of compounds **5**, **Pc-6**, **Pc-7** and **Pc-8**.

[M+4H]⁺ for **Pc-7** and 1487.28 as the [M+K]⁺. In the mass spectra of phthalocyanines the presence of the molecular ion peaks at m/z = 1477.65 [M+Na]⁺, 1452.36 [M+4H]⁺ and 1487.28 [M+K]⁺ respectively, clearly indicates the formation of the designed structures in **Scheme 1**.

3.3. UV-Vis absorption spectra

The UV-Visible spectra of **Pc-6**, **Pc-7** and **Pc-8** was recorded by using chloroform as solvent over a wide range concentration between 10^{-5} and 10^{-4} M. The electronic absorption spectra of phthalocyanines can be seen in **Fig. 5** (a), (b) and (c) for **Pc-6**, **Pc-7** and **Pc-8** respectively in the range of 300–800 nm. The typical Soret bands around 350 nm are seen for all of the MPC's in **Fig. 5**. The non-aggregation behavior of phthalocyanines is seen from the figures. The electronic absorption spectra figures show typical non-aggregated phthalocyanines. But, aggregation may occur as high concentrations are reached. This is also evident in electrochemical measurements. The insets in **Fig. 5** which are seen as an almost linear lines, gave linear regression coefficients of 0.9819, 0.961 and 0.9957 for phthalocyanines **Pc-6**, **Pc-7** and **Pc-8**. **Fig. 5** (a) shows that **Pc-6** has a strong Q band at 708 nm in chloroform having a shoulder at 648 nm with a vibronic band at 624 nm and also a Soret band peaking at 360 nm. The **Fig. 5** (b) shows that **Pc-7** has also a Q band at 680 nm in chloroform having a shoulder at 616 and also a Soret band peaking at 332 nm. On the other side **Fig. 5** (c) shows that **Pc-8** has a Q band at 616 nm with a shoulder at 672 nm and also has a Soret band peaking at 332 nm.

Table 2
Hydrogen-bond geometry.

D—H...A	D—H (Å)	H...A (Å)	D...A (Å)	D—H...A (°)
C10'-H10'A...N3 ⁱ	0.99	2.48	3.461	170
C10'-H10'B...N5 ⁱⁱ	0.99	2.51	3.415	151
C16-H16...S1 ⁱⁱⁱ	0.95	2.85	3.698	150
C8'-H8'...N2 ⁱ	0.95	2.44	3.242	142
C10-H10A...N3 ^{iv}	0.99	2.52	3.490	166
C10-H10B...N5 ^v	0.99	2.51	3.452	158
C8-H8...N2 ^{iv}	0.95	2.34	3.206	151
C7-H7B...N3 ⁱⁱⁱ	0.99	2.59	3.394	139
C7'-H7'B...N3 ^{vi}	0.99	2.58	3.491	153

Symmetry codes: (i) x, y+1, z; (ii) x+1, -y, z-1/2; (iii) x-1, y+1, z; (iv) x, y-1, z; (v) x, -y+2, z+1/2; (vi) x+1, y-1, z.

As can be clearly seen from the inset graphics in **Fig. 5** that all of the phthalocyanines, **Pc-6**, **Pc-7** and **Pc-8**, show non-aggregation behaviour in the concentration range 10^{-5} and 10^{-4} M. That is to say, they all have very good solubility in chloroform, which is an organic solvent. All of three Pcs are able to use for appropriate applications. So, the application studies should be performed with these phthalocyanines.

3.4. Results of X-ray diffraction experiment of compound **5**, ($C_{18}H_{13}N_5OS$)

A monoclinic (Pc) single crystal of the compound **5** has formed with the unitcell parameters of $a = 11.7491$ Å, $b = 5.4135$ Å, $c = 26.1548$ Å, and $\beta = 99.719^\circ$. While four molecules are forming the unit-cell, two of them have created the asymmetric unit unit. **Fig. 6** presents the atomic arrangement for the asymmetric unit with the atomic labels and the gravity centres (Cg). For clarity, the hydrogen atom labels were not provided in the figure. But the hydrogen atoms have been labelled as the same numbers as the carbon atoms to which they are bounded (like C4—H4).

Molecule Description: The asymmetric unit contains no H...H intra-molecular interaction within the possible Van der Waals ranges. For the asymmetric unit, there are six rings observed as shown in the **Fig. 6** (a). Two of them were five-membered rings and rest of them six-membered rings. Here the five membered rings **A** (N1-N2-N3-C9-C8) and **A'** (N1'-N2'-N3'-C9'-C8'), and the six membered rings **B** (C1—C6), **B'** (C1'—C6'), **C** (C11—C16), and **C'**(C11'—C16') exhibited perfect mean planes with the RMS values of 0.00186 Å, 0.00126 Å, 0.0037 Å, 0.0102 Å, 0.0088 Å, and 0.0037 Å, respectively. For the **molecule 1** of asymmetric unit, a 68.34° dihedral angle has been observed between the rings **A** and **B**, while it was 66.83° between the **A** and **C**. The phenyl and triazole groups bonded together via S1 atom with a bond angle of 100.11° (C1—S1—C7). Where the bond lengths are C1—S1= 1.79 Å and S1—C9= 1.80 Å. Besides, the phthalonitrile is bonded to triazole group via O1 atom with a bond angle of 117.97° (C10—O1—C11), where the bond lengths are C10—O1= 1.45 Å and O1—C11=1.35 Å. The **molecule 2** exhibited slightly different geometric properties than **molecule 1** such as the dihedral angle between the rings **A'** and **B'** is 60.22° , and between the rings **A'** and **C'** is 68.95° . Furthermore, very similar bond angles of 101.10° (C1'—S1'—C7') and 117.52° (C10'—O1'—C11') have been observed with the similar bond lengths of C1'—S1'=1.78 Å, S1'—C7'= 1.80 Å, C10'—O1'= 1.44 Å, and O1'—C11'=1.36 Å.

Supramolecular Dynamics: **Fig. 6** (b) presents the monoclinic molecular assembly of compound **5** with the unitcell through the (010) view. Here the solid-stated crystal structure has been stabilized by the domination of D—H...A, Cg...Cg and Y—X...Cg intermolecular interactions. All these possible interactions have been listed in the **Table 2**, **Table 3**, and **Table 4**, respectively. In addition to the hydrogen bonds (D—H...A), the Cg...Cg interactions be-

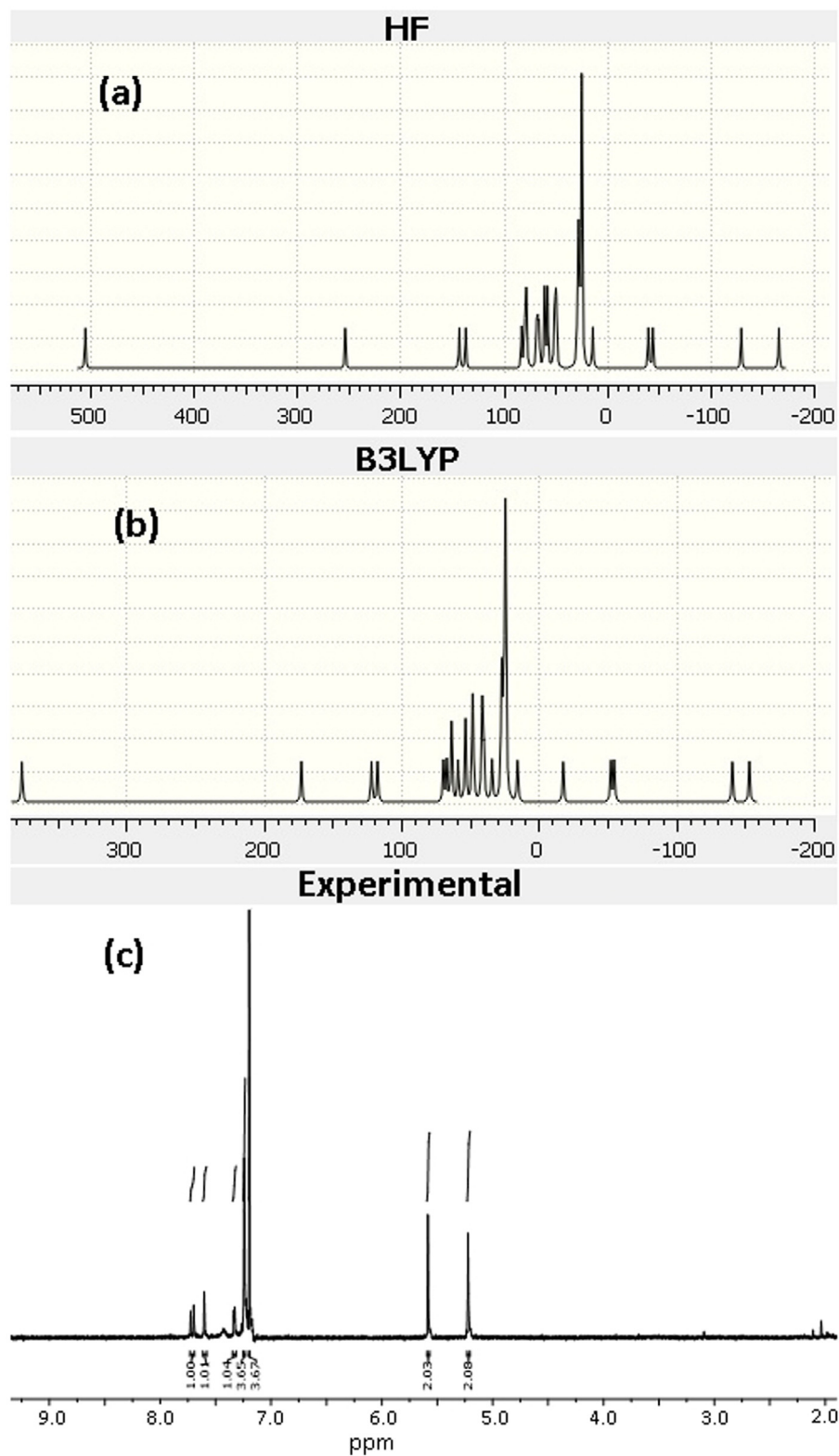


Fig. 3. (a) HF, (b) B3LYP and (c) experimental calculated NMR spectra of compound **5**.

tween six-membered rings have contributed to stabilize the crystal structure along b-axis while the Cg...Cg interactions between five-membered rings have contributed to stabilization along a-c plane.

In order to visualize the intermolecular interactions and quantify the percentages of interactions present in the crystal structure of compound **5**, the Hirshfeld surface analysis of the asymmetric

unit has been done by using the "Crystalexplorer17" software [117]. Fig. 7 (a) presents the Hirshfeld surfaces in two different views with the "**dnorm**", "**shape index**" and "**curvedness**" modes. The red zones on the **dnorm** show where the strongest intermolecular interactions are. Besides, the coloured surfaces provided by the **shape index** is mapping the Cg...Cg interactions via the adjacent

Table 3
The inter-molecular $\pi\cdots\pi$ ($Cg\cdots Cg$) interactions.^a

No	$Cg(I)\cdots Cg(J)$	Symmetry	$Cg\cdots Cg$ ^b	$Cg(I)\text{-perp}$ ^c	$Cg(J)\text{-perp}$ ^d	α ^e
1	$Cg(1)\cdots Cg(2)$	x, y, z	4.628	3.542	3.852	68.3
2	$Cg(1)\cdots Cg(1')$	x-1, y, z	5.014	3.898	3.049	14.4
3	$Cg(1)\cdots Cg(1')$	x-1, y+1, z	4.068	3.004	3.508(3)	14.4
4	$Cg(1)\cdots Cg(2')$	x, y, z	5.935	1.224	4.851	68.4
5	$Cg(1)\cdots Cg(2')$	x, y+1, z	5.361	1.769	4.393	68.4
6	$Cg(2)\cdots Cg(2)$	x, y-1, z	5.413	2.765	2.765	0.0
7	$Cg(2)\cdots Cg(2')$	x, y+1, z	5.140	1.394	4.550	64.6
8	$Cg(2)\cdots Cg(3')$	x, y, z	4.131	3.415	3.592	13.1
9	$Cg(3)\cdots Cg(1)$	x, y-1, z	5.918	2.388	3.793	66.8
10	$Cg(3)\cdots Cg(3)$	x, y-1, z	5.413	3.257	3.258	0.0
11	$Cg(3)\cdots Cg(2')$	x-1, y, z	5.958	0.031	4.633	87.8
12	$Cg(1')\cdots Cg(2)$	x, y-1, z	5.368	0.898	4.912	76.5
13	$Cg(1')\cdots Cg(2')$	x, y, z	5.657	1.867	4.018	76.5
14	$Cg(1')\cdots Cg(2')$	x, y, z	4.787	3.569	3.700	60.2
15	$Cg(2')\cdots Cg(2)$	x, y, z	5.244	1.785	4.385	64.6
16	$Cg(2')\cdots Cg(2')$	x, y-1, z	5.414	2.991	2.991	0.0
17	$Cg(2')\cdots Cg(3')$	x, y-1, z+1/2	5.151	3.399	3.777	6.3
18	$Cg(3')\cdots Cg(3')$	x, y-1, z	5.413	3.276	3.276	0.0

^a $Cg\cdots Cg < 6.0 \text{ \AA}$. ^b Distances between centroids of the rings. ^c Perpendicular distance of $Cg(I)$ on ring J plane (\AA). ^d Perpendicular distance of $Cg(J)$ on ring I plane (\AA). ^e Dihedral angle between planes I and J ($^\circ$).

Table 4
Inter-molecular Y-X...Cg interactions.^a

Y-X...Cg(I)	Symmetry	X...Cg(I) ^b	X-perp ^c	Y-X...Cg ^d	Y...Cg ^e
C17-N4...Cg(3)	x, y-1, z	3.609	3.431	89.6	3.777
C17'-N4'...Cg(3')	x, y+1, z	3.532	3.397	91.5	3.741
C18'-N5'...Cg(2')	x, y-1, z+1/2	3.556	3.419	85.0	3.637

^a $Cg\cdots Cg < 4.0 \text{ \AA}$. ^b Distance from X atom to Cg (I). ^c Perpendicular distance from X atom to ring plane. ^d Angle between Y-X...Cg(I) ($^\circ$). ^e Distance from Y atom to Cg(I). All distances have been represented as in the unit of \AA .

blue and red triangles. **Curvedness** image visualize the relatively flat surfaces.

The 2D fingerprint plots given in Fig. 7 (b) indicate that the N...H / H...N (37.3 %) contact (C-H...N) is the major contributor for the Hirshfeld surface while the H...H (19.3 %), C...H / H...C (17.5%), C...N / N...C (5.7%, C-N...Cg), S...H / H...S (4.9%), and O...H / H...O (4.1%) contacts are making less significant contributions. Because of the $\pi\cdots\pi$ interactions in the crystal structure, there is a contribution of C...C (3.8%). And the other contacts are making very small contributions such as S...N / N...S (2.3%), N...N (2.0%), C...S / S...C (1.8%), C...O / O...C (1.1%), and O...S / S...O (0.2%).

3.5. Quantum Chemical Calculations

We need the quantum chemical parameter to understand the reaction mechanism. The frontier molecular orbitals HOMO and LUMO, and also ΔE (band gap; energy difference between HOMO and LUMO) are very important for molecular activity. HOMO is the Highest Occupied Molecular Orbital and LUMO is the Lowest Unoccupied Molecular Orbital. The obtained results are shown in Table 5.

HOMO and LUMO tells us from which region of the molecule it reacts. Energy level of the HOMO is related to the tendency of donating electron. If a molecule has higher energy level of the HOMO that would give electron. On the other side, energy level of the LUMO is related to the tendency of accepting electron. If a molecule has lower energy level of the LUMO, that would accept electron. So higher level of the HOMO and lower level of the LUMO give molecule higher activity.

Chemical hardness, η , is resistance to polarization of electron cloud. Chemical hardness allows the ligand to react with metal ions of the same hardness level. This gives information about the

Table 5
The quantum chemical parameters of compound 5 calculated with HF and B3LYP 6.311+G(d, (eV)).4.

	Compound 5	
	HF	B3LYP
E_{HOMO}	-9,73134	-7,16585
E_{LUMO}	0,71539	-2,39215
Band Gap, ΔE	10,44673	4,77370
Global softness, σ	0,19145	0,41896
Global electrophilicity, ω	1,94528	4,78431
Ionization potential, I	9,73134	7,16585
Electron affinity, A	-0,71539	2,39215
Chemical hardness, η	5,22336	2,38685
Electronegativity, χ	4,50798	4,77900

reactivity of the ligand. As known both global softness, σ , and chemical hardness are explained using the energy value of HOMO and LUMO [118].

$$\eta = \frac{E_{LUMO} - E_{HOMO}}{2} = \left(\frac{I - A}{2} \right) \quad (1)$$

$$\sigma = \frac{1}{\eta} \quad (2)$$

The chemical potential of a system, μ , is defined as the derivative of energy in equilibrium by the number of electrons in fixed molecular geometry.

$$\mu = \frac{E_{HOMO} + E_{LUMO}}{2} \quad (3)$$

Electronegativity, χ , is negative of the chemical potential in Eq. (4). The global electrophilicity index (ω) is calculated via

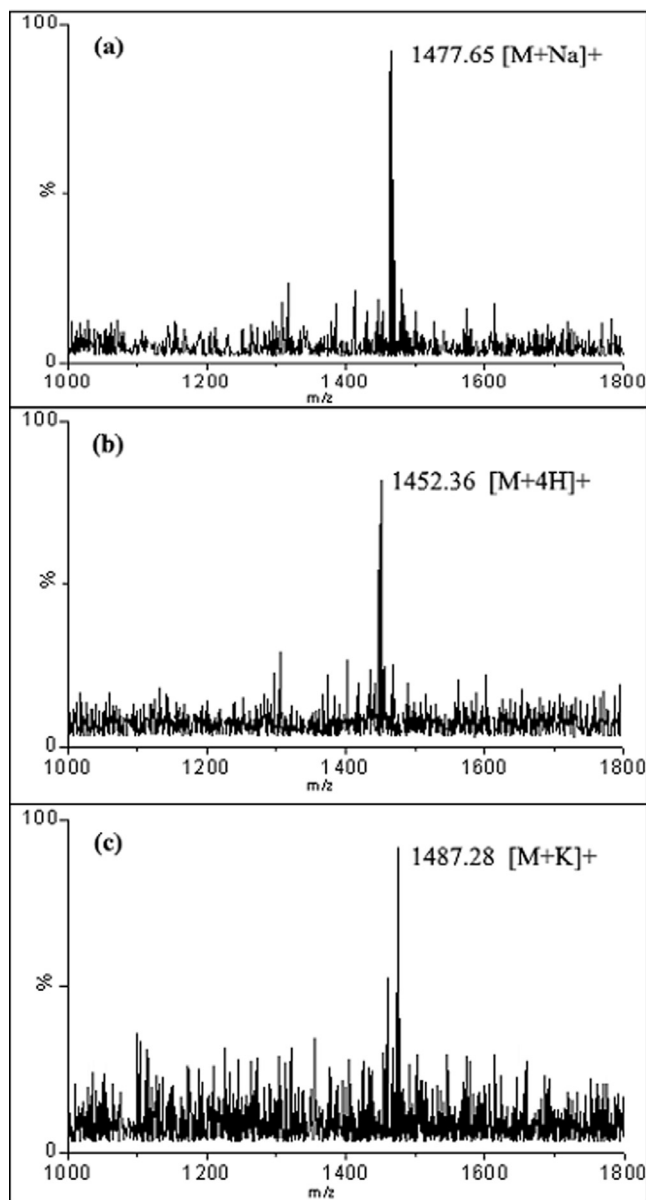


Fig. 4. Mass spectra of (a) **Pc-6**, (b) **Pc-7** and (c) **Pc-8**.

Eq. (5).

$$\chi = -\mu = \left(\frac{I+A}{2} \right) \quad (4)$$

$$\omega = \frac{\chi^2}{2\eta} \quad (5)$$

Fig. 8 shows HOMO, LUMO, ESP and the optimized geometric structures of compound **5**. The shape of ESP shows on which atom has more density of electrons on the surface of compound.

3.6. Electrochemical measurements

The voltammograms were recorded by using Parstat 2273 potentiostat/galvanostat. Pt as working electrode, Pt as counter electrode and an Ag/AgCl as reference electrode were used in a three electrodes system. Extra pure dimethylsulfoxide as solvent was used for electrochemical measurements and 0,1 mol/L tetra-n-butylammoniumtetrafluoroborate as the supporting electrolyte ($TBABF_4$, 99%) was used. Voltammetric studies were performed in

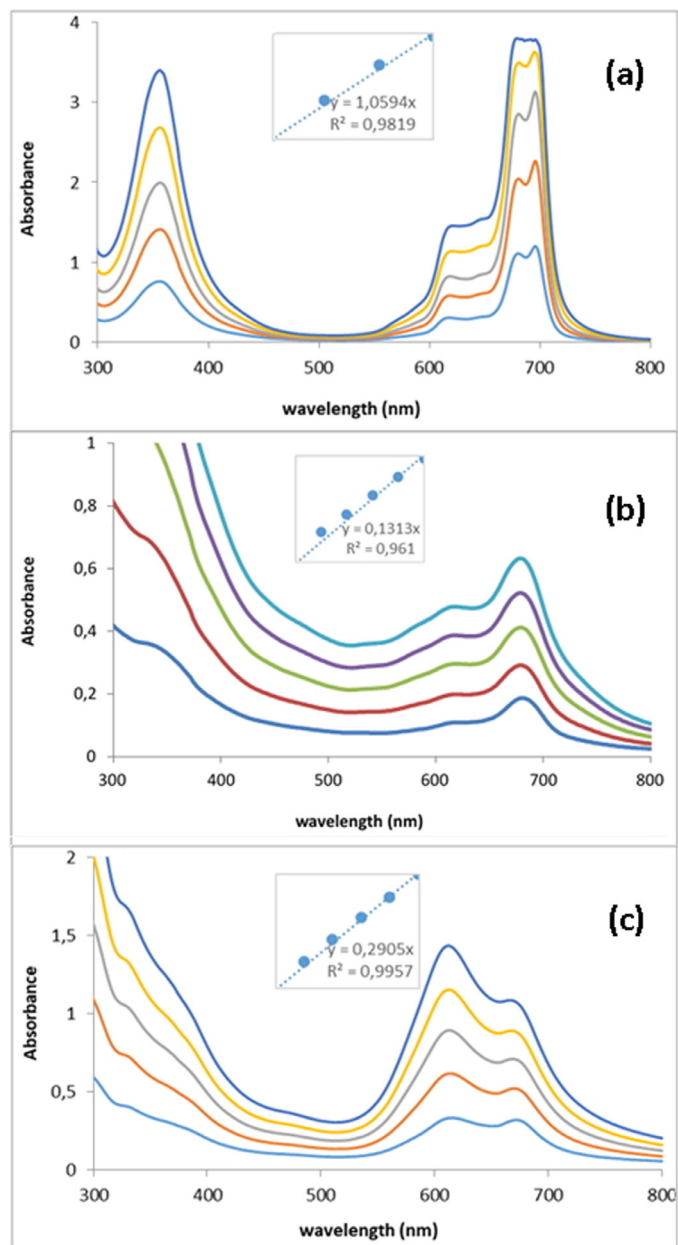


Fig. 5. UV-Visible absorption spectra of (a) Zinc phthalocyanine, **Pc-6**, (b) Cobalt (II) phthalocyanine, **Pc-7**, (c) Nickel (II) phthalocyanine, **Pc-8**.

two electrochemical techniques. One is cyclic voltammetry (CV) and second is square wave voltammetry.

The left column of the **Fig. 9** shows CV voltammograms and the right column of **Fig. 9** shows square wave voltammograms in DMSO/ $TBABF_4$ for metallophthalocyanines. When the cyclic voltammetry study of **Pc-6** compound was examined on the left column of **Fig. 9** (a) it appears to give a reversible reduction pair called as R_1 which has $E_{1/2}$ value as -1.31 V and a non-reversible reduction called as R_2 which has $E_{1/2}$ value as -1.73 V. During the anodic potential screening of the same complex, one non-reversible oxidation peak called as O_1 which has $E_{1/2}$ value as 0.84 V and one anodic oxidation peak called as O_2 which has $E_{1/2}$ value as 1.52 V were determined. When the cyclic voltammetry study of **Pc-7** compound was examined on the left column of **Fig. 9** (b) it appears to give a reversible reduction pair called as R_1 which has $E_{1/2}$ value as -0.57 V and a reversible oxidation peak called as O_1 which has $E_{1/2}$ value as 1.45 V. When the cyclic voltammetry study

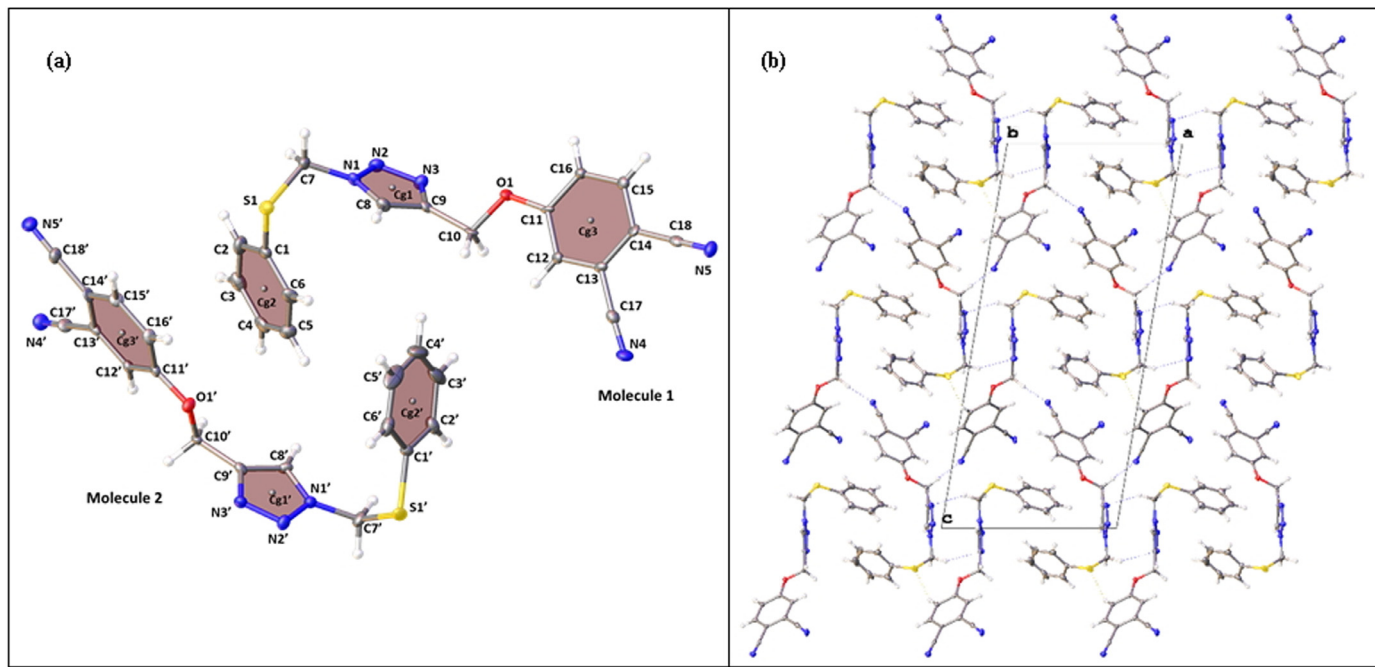


Fig. 6. (a) The atomic arrangement with atomic labels for the asymmetric unit of compound **5**. There are two molecules in the asymmetric unit. While the N1–N2–N3–C9–C8 atoms are exhibiting a five membered ring **A**, C1–C6 and C11–C16 atoms are exhibiting six-membered rings **B** and **C**, respectively. Where, Cg1 is the gravity centre (Cg) of the five membered ring **A**, Cg2 and Cg3 represent the gravity centres for the six membered rings **B** and **C**, respectively. (b) The monoclinic molecular assembly of compound **5** through the (010) view. Dashed dots indicate the Hydrogen bonds (H...A).

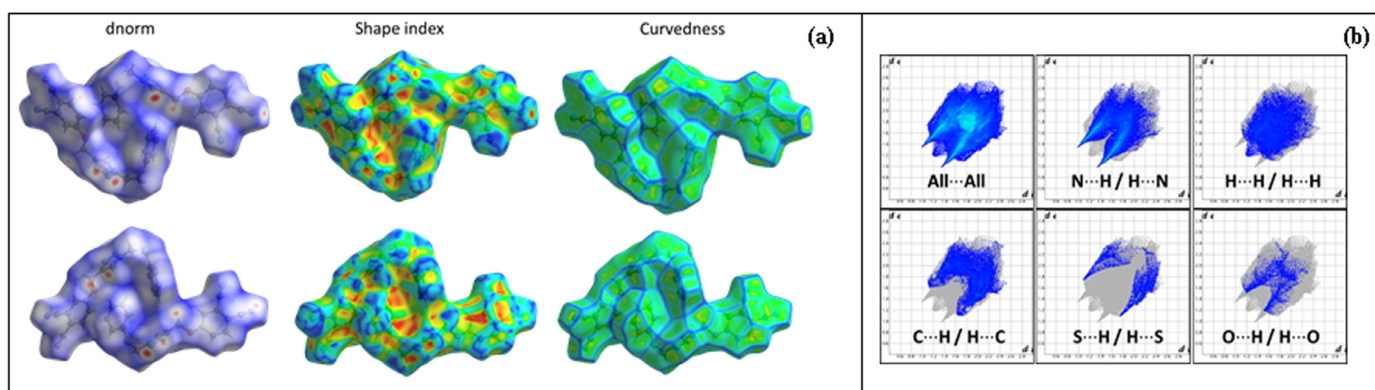


Fig. 7. (a) The Hirshfeld surfaces in 3D that showing the intermolecular interactions (**d_{norm}**), Cg...Cg interactions (**shape index**) and relatively flat surfaces (**curvedness**). (b) A view of 2D fingerprint plot for the asymmetric unit of the compound **5**. Here the C–H...N contact is the major contributor to the Hirshfeld surface.

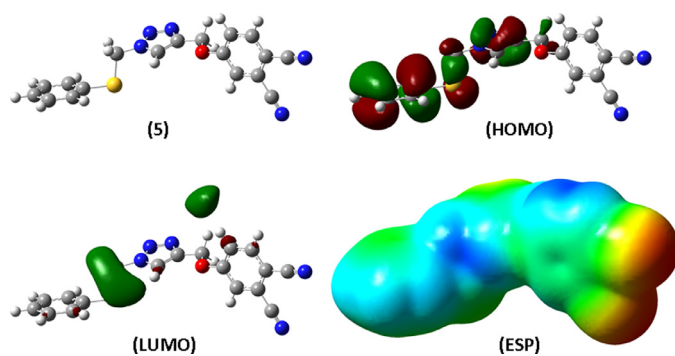


Fig. 8. HOMO, LUMO, ESP and the optimized geometric structures of compound **5**.

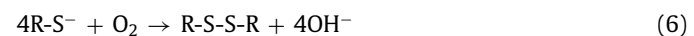
of **Pc-8** compound was examined on the left column of Fig. 9 (c) it appears to give a reversible reduction pair called as R₁ which has E_{1/2} value as -0.88 V and a reversible oxidation peak called as O₁

which has E_{1/2} value as 1.80 V. Cyclic voltammetric results of synthesized phthalocyanines were supported by square wave voltammetry as it is seen on the right column of Fig. 9 (a), (b) and (c).

3.7. Catalytic oxidation of 2-mercaptopethanol

The catalytic activity of Co(II)phthalocyanines on the oxidation of 2-mercaptopethanol is a highly studied application in the literature. **Pc-7**, Co(II)phthalocyanine, coordinates to the thiolate anion RS⁻ generated by NaOH and O₂ on two axial sides of the central Co(II) in **Pc-7** [48–50]. At this coordinating time, an electron transfer reaction occurs from the thiol to oxygen via the central Co(II). The resulting thiol radicals combine to form disulfide. Thus, thiol compounds are converted to more passive disulfides by this oxidation reaction and lose their reactivity.

Equation (6) shows the reaction between 2-mercaptopethanol and oxygen.



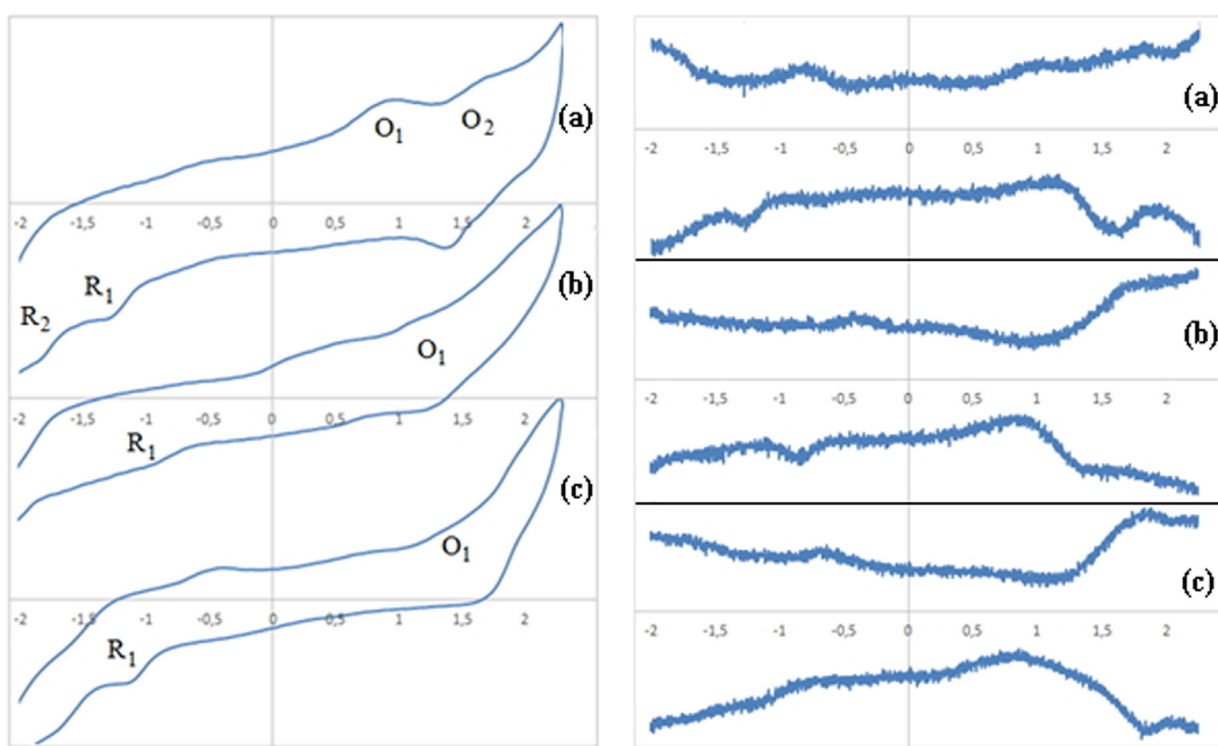


Fig. 9. Cyclic voltammograms of (a) **Pc-6**, (b) **Pc-7** and (c) **Pc-8** on the left and Square wave voltammograms of (a) **Pc-6**, (b) **Pc-7** and (c) **Pc-8** on the right.

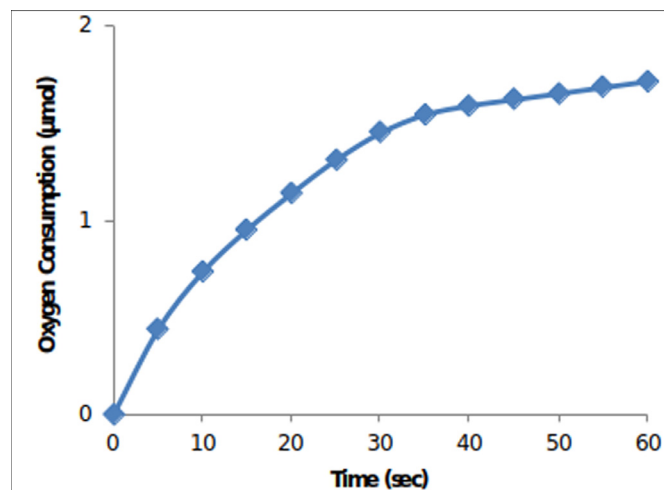


Fig. 10. Oxygen consumption in the reaction of catalytic oxidation of 2-mercaptopropanoic acid by $\text{Co}(\text{II})$ -phthalocyanine as catalyst.

The ratio of 2-mercaptopropanoic acid and phthalocyanine is 5500:1. This thiol/catalyst ratio is also quite good in terms of catalytic work. Yong Pan and others used the ratio of 2-mercaptopropanoic acid and phthalocyanine was 5000:1 [119]. When NaOH solution is added, thiol (RSH) will lose proton and convert to thiol (RS^-). The reaction therefore needs a basic environment. $\text{Co}(\text{II})$ -phthalocyanine will then begin to catalyze the oxidation reaction of 2-mercaptopropanoic acid with oxygen. TON, initial rate of reaction and oxygen consumption were calculated respectively as 18.09, 0.12 $\mu\text{mol.s}^{-1}$, 6.88 $\mu\text{mol.min}^{-1}$ and change in oxygen consumption over time is shown in Fig. 10.

4. Conclusion

As a result, novel Zn (II), Co (II) and Ni (II) phthalocyanines were synthesized carrying four triazole groups at peripheral positions. The well-known **Pc** synthesize method was used for the direct synthesize of **Pc-6**, **Pc-7** and **Pc-8** phthalocyanines. The alkyne compound, **3**, was obtained by reaction of 4-nitrophthalonitrile and propargyl alcohol in the presence of potassium carbonate at room temperature. This compound was reacted with azidomethyl phenyl sulfite, **4**, under the catalysis of copper (II) sulfate penta hydrate and sodium ascorbate to give a triazole compound which was the click product. The structures of all synthesized compounds have been fully characterized by combining FT-IR, ^1H NMR, ^{13}C NMR, MALDI-TOF MS, UV-vis spectroscopy and elemental analysis techniques. Electronic absorption spectra have shown that all phthalocyanines are non-aggregated molecules. Cyclic voltammograms give two reduction reactions and two oxidation reactions for **Pc-6**. On the other hand, one reduction reaction and one oxidation reaction for **Pc-7** and **Pc-8**. The catalytic properties of **Pc-7**, cobalt(II)phthalocyanine, were investigated in the oxidation reaction of 2-mercaptopropanoic acid with oxygen. Catalytic oxidation of 2-mercaptopropanoic acid is a widely investigated reaction for the determination of catalytic activity of phthalocyanines. Turnover number, initial reaction rate and the oxygen consumption was found in the catalytic oxidation of 2-mercaptopropanoic acid as 18.09, 0.12 $\mu\text{mol.s}^{-1}$, 6.88 $\mu\text{mol.min}^{-1}$ respectively.

Declaration of Competing Interest

The authors declare that they have no known competing financial interests or personal relationships that could have appeared to influence the work reported in this paper.

CRediT authorship contribution statement

Hüseyin Karaca: Conceptualization, Funding acquisition, Investigation, Methodology, Software, Validation, Visualization, Writing - original draft, Writing - review & editing. **Nagihan Çaylak Delibaş:** Conceptualization, Supervision. **Serap Sağlam:** Writing - original draft. **Hasan Pişkin:** Methodology, Writing - original draft. **Serdar Sezer:** Conceptualization, Supervision. **Tuncer Hökelek:** Conceptualization, Supervision. **Murat Teker:** Supervision.

Acknowledgments

This research is funded by Sakarya University Scientific Research Projects Unit (BAPK: 2018-3-12-165).

References

- [1] C.C. Leznoff, A.B.P. Lever, *Phthalocyanines, properties and applications*, 1-4, VCH, New York, 1989 1992, 1993, 1996.
- [2] The Porphyrin Handbook: Phthalocyanines: Spectroscopic and Electrochemical Characterization: 16, Kadish, Karl; Guilard, Roger; Smith, Kevin M. ed., Academic Press, San Diego, 2003.
- [3] H.P. Karaoglu, A. Atsay, I. Nar, V. McKee, M.B. Koçak, E. Hamuryudan, A. Güll, Near-infrared absorbing π -extended hexadeca substituted phthalocyanines, *Journal of Molecular Structure* 1197 (2019) 736–741.
- [4] Z. Şen, D.K. Tarakci, I. Gürol, V. Ahsen, M. Harbeck, Governing the sorption and sensing properties of titanium phthalocyanines by means of axial ligands, *Sensors and Actuators B: Chemical* 229 (2016) 581–586.
- [5] M. Özer, A. Altindal, A.R. Özka, M. Bulut, Ö. Bekaroğlu, Synthesis, characterization, and electrical, electrochemical and gas sensing properties of a novel cyclic borazine derivative containing three phthalocyanato zinc(II) macrocycles, *Synthetic Metals* 155 (1) (2005) 222–231.
- [6] M. Hanack, M. Fiedler, L.R. Subramanian, Phthalocyanatoiron complexes with tridentate ligands, *Synthetic Metals* 100 (1) (1999) 123–130.
- [7] M. Urbani, M.E. Ragoussi, M.K. Nazeeruddin, T. Torres, Phthalocyanines for dye-sensitized solar cells, *Coordination Chemistry Reviews* 381 (2019) 1–64.
- [8] A. Sindelo, N. Kobayashi, M. Kimura, T. Nyokong, Physicochemical and photodynamic antimicrobial chemotherapy activity of morpholine-substituted phthalocyanines: Effect of point of substitution and central metal, *Journal of Photochemistry and Photobiology A: Chemistry* 374 (2019) 58–67.
- [9] K. Lewandowska, D. Wróbel, A. Biadasz, R. Świertlik, Nanolayers of selected porphyrin and phthalocyanine dyes on solid substrates studied by electronic absorption and IR reflection-absorption spectroscopy, *Journal of Photochemistry and Photobiology A: Chemistry* 200 (Issues 2–3) (2008) 225–231.
- [10] F. Harrelkas, A. Paulo, M.M. Alves, L. El Khadir, O. Zahraa, M.N. Pons, F.P. van der Zee, Photocatalytic and combined anaerobic-photocatalytic treatment of textile dyes, *Chemosphere* 72 (11) (2008) 1816–1822.
- [11] D.S. Nesterov, O.V. Nesterova, M.N. Kopylovich, A.J.L. Pombeiro, Pronounced retention of stereoconfiguration upon sp³ CH bonds hydroxylation of dimethylcyclohexanes and decahydronaphthalenes with m-CPBA oxidant and a Co-phthalocyanine catalyst, *Molecular Catalysis* 459 (2018) 8–15.
- [12] S. Farahmand, M. Ghiasi, J.S. Razavizadeh, Copper phthalocyanine as an efficient and reusable heterogeneous catalyst for direct hydroxylation of benzene to phenol under mild conditions, *Inorganica Chimica Acta* 484 (2019) 174–179.
- [13] M.T. Noori, N. Verma, Cobalt – Iron phthalocyanine supported on carbide – Derived carbon as an excellent oxygen reduction reaction catalyst for microbial fuel cells, *Electrochimica Acta* 298 (2019) 70–79.
- [14] M. Passard, A. Pauly, J.P. Blanc, S. Dogo, J.P. Germain, C. Maleysson, Doping mechanisms of phthalocyanines by oxidizing gases: Application to gas sensors, *Thin Solid Films* 237 (1–2) (1994) 272–276.
- [15] Y. Açıkbaba, M. Evyapan, T. Ceyhan, R. Çapan, Ö. Bekaroğlu, Characterization and organic vapor sensing properties of Langmuir–Blodgett film using a new three oxygen-linked phthalocyanine incorporating lutetium, *Sensors and Actuators B: Chemical* 135 (2) (2009) 426–429.
- [16] Z.J. Guoa, B. Wang, Wang X, Y. Lia, S. Gaia, Y. Wu, X.L. Cheng, A high-sensitive room temperature gas sensor based on cobalt phthalocyanines and reduced graphene oxide nanohybrids for the ppb-levels of ammonia detection, *RSC Advances* 9 (2019) 37518–37525.
- [17] F. Zina, N.M. Nooredeen, S. Azzouzi, M. Ben Ali, M.N. Abbas, A. Errachid, Novel Sensitive Impedimetric Microsensor for Phosphate Detection Based on a Novel Copper Phthalocyanine Derivative, *Analytical Letters* 51 (3) (2018) 371–386.
- [18] Z. Shaghaghi, R. Rezanezhad, New Chloro-Based Azo-Azomethine Dyes: Synthesis, Biological and Optical Spectroscopic Studies for Detection of some Transition Metal Ions, *ChemistrySelect* 3 (20) (2018) 5534–5540.
- [19] H. Wang, T. Fukuda, N. Ishikawa, Y. Matsuo, Solvent-dependent morphology of thermally converted copper phthalocyanine for solution-processed small molecule organic photovoltaic devices, *Organic Electronics* 15 (1) (2014) 139–143.
- [20] G.D. Sharma, P. BalaRaju, M.S. Roy, Effect of functional groups of acceptor material on photovoltaic response of bulk hetero-junction organic devices based on tin phthalocyanine (SnPc), *Solar Energy Materials and Solar Cells* 92 (3) (2008) 261–272.
- [21] G.Ö. Artuç, A. Altindal, B.B. Eran, M. Bulut, Synthesis, characterization and photovoltaic behaviours of peripheral and non-peripheral tetra-[4-(4-octylpiperazin-1-yl)phenoxy] substituted zinc(II), cobalt(II), copper(II) and indium(III) phthalocyanines, *Inorganica Chimica Acta* 490 (2019) 35–44.
- [22] A. Günel, E. Güzel, A.T. Bilgiçli, İ. Şişman, M.N. Yarasir, Synthesis of non-peripheral thioanisole-substituted phthalocyanines: Photophysical, electrochemical, photovoltaic, and sensing properties, *Journal of Photochemistry and Photobiology A: Chemistry* 348 (2017) 57–67.
- [23] J. Szostak, G. Jarosz, R. Sigerski, Photovoltaic properties of cadmium selenide-titanyl phthalocyanine planar heterojunction devices, *Chemical Physics* 456 (2015) 57–60.
- [24] Y. Ohmori, E. Itoh, K. Miyairi, Photovoltaic properties of phthalocyanine based p-n diode evaporated onto titanium dioxide, *Thin Solid Films* 499 (1–2) (2006) 369–373.
- [25] C. Solis, E. Baigorria, M.E. Milanesio, G. Morales, E.N. Durantini, L. Otero, M. Gervaldo, Electrochemical polymerization of EDOT modified Phthalocyanines and their applications as electrochromic materials with green coloration, and strong absorption in the Near-IR, *Electrochimica Acta* 213 (2016) 594–605.
- [26] P. Şen, F. Dumludag, B. Salih, A.R. Özka, Ö. Bekaroğlu, Synthesis and electrochemical, electrochromic and electrical properties of novel s-triazine bridged trinuclear Zn(II), Cu(II) and Lu(III) and a tris double-decker Lu(III) phthalocyanines, *Synthetic Metals* 161 (13–14) (2011) 1245–1254.
- [27] A. Ghoochian, F. Tavoli, N. Alizadeh, Long-term stability of nanostructured polypyrrrole electrochromic devices by using deep eutectic solvents, *Journal of Electroanalytical Chemistry* 807 (2017) 70–75.
- [28] P.R. Somani, S. Radhakrishnan, Electrochromic materials and devices: present and future, *Materials Chemistry and Physics* 77 (1) (2003) 117–133.
- [29] T. Basova, A.G. Gürek, V. Ahsen, A. Ray, Electrochromic lutetium phthalocyanine films for in situ detection of NADH, *Optical Materials* 35 (3) (2013) 634–637.
- [30] S. Gorduk, Synthesis, photophysics and photochemistry studies on non-peripherally tetra-substituted Zn(II) and In(III) phthalocyanines bearing ferulic acid units, *Journal of Molecular Structure* 1198 (2019) 126921.
- [31] J. Silver, P.J. Lukes, P.K. Hey, J.M. O'Connor, The electrochromic behaviour of zirconium diphthalocyanine and molybdenum phthalocyanine oxide, *Polyhedron* 8 (13–14) (1989) 1631–1635.
- [32] S. Belali, H. Savoie, J.M. O'Brien, A.A. Cafolla, B. O'Connell, A.R. Karimi, R.W. Boyle, M.O. Senge, Synthesis and Characterization of Temperature-Sensitive and Chemically Cross-Linked Poly(N-isopropylacrylamide)/Photosensitizer Hydrogels for Applications in Photodynamic Therapy, *Biomacromolecules* 19 (5) (2018) 1592–1601.
- [33] B.M. Motloung, K.E. Sekhosana, M. Managa, E. Prinsloo, T. Nyokong, The photophysicochemical properties and photodynamic therapy activity of phenyldiazenyl phenoxy substituted phthalocyanines when incorporated into Pluronic® F127 micelles, *Polyhedron* 174 (2019) 114157.
- [34] P. Sen, M. Managa, T. Nyokong, New type of metal-free and Zinc(II), In(III), Ga(III) phthalocyanines carrying biologically active substituents: Synthesis and photophysicochemical properties and photodynamic therapy activity, *Inorganica Chimica Acta* 491 (2019) 1–8.
- [35] C.Y. Boyar, M. Çamur, Novel water soluble 7-oxy-4-(pyridine-3-yl)coumarin substituted phthalocyanines as potential photosensitizers for photodynamic therapy, *Inorganica Chimica Acta* 494 (2019) 30–41.
- [36] E. Güzel, A. Günsel, A.T. Bilgiçli, G.Y. Atmaca, M.N. Yarasir, Synthesis and photophysicochemical properties of novel thiadiazole-substituted zinc (II), gallium (III) and silicon (IV) phthalocyanines for photodynamic therapy, *Inorganica Chimica Acta* 467 (2017) 169–176.
- [37] R.G. de Lima, A.C. Tedesco, R.S. da Silva, M.J. Lawrence, Ultra deformable liposome loaded with zinc phthalocyanine and [Ru(NH₂NHq)(tpy)NO]³⁺ for photodynamic therapy by topical application, *Photodiagnosis and Photodynamic Therapy* 19 (2017) 184–193.
- [38] J. Ma, D. Chen, Y. Li, Y. Chen, Q. Liu, X. Zhou, K. Qian, Z. Li, H. Ruan, Z. Hou, X. Zhu, Zinc phthalocyanine-soybean phospholipid complex based drug carrier for switchable photoacoustic/fluorescence image, multiphase photothermal/photodynamic treatment and synergistic therapy, *Journal of Controlled Release* 284 (2018) 1–14.
- [39] F. Navaeipour, H. Afsharan, H. Tajallii, M. Mollabashi, F. Ranjbari, A. Montaseri, M.R. Rashidi, Effects of continuous wave and fractionated diode laser on human fibroblast cancer and dermal normal cells by zinc phthalocyanine in photodynamic therapy: A comparative study, *Journal of Photochemistry and Photobiology B: Biology* 161 (2016) 456–462.
- [40] K. Ocakoglu, O. Rr, O.A. Ersoz, F.Y. Lambrecht, M. Ince, C. Kayabasi, C. Gunduz, Evaluation of nuclear imaging potential and photodynamic therapy efficacy of symmetrical and asymmetrical zinc phthalocyanines, *Journal of Drug Delivery Science and Technology* 33 (2016) 164–169.
- [41] F. Bayat, A.R. Karimi, Design of photodynamic chitosan hydrogels bearing phthalocyanine-colistin conjugate as an antibacterial agent, *International Journal of Biological Macromolecules* 129 (2019) 927–935.

- [42] M. Camerin, M. Magaraggia, M. Soncin, G. Jori, M. Moreno, I. Chambrier, M.J. Cook, D. A.Russell, The in vivo efficacy of phthalocyanine-nanoparticle conjugates for the photodynamic therapy of amelanotic melanoma, *European Journal of Cancer* 46 (10) (2010) 1910–1918.
- [43] K. Sakamoto, T. Kato, E. Ohno-Okumura, M. Watanabe, M.J. Cook, Synthesis of novel cationic amphiphilic phthalocyanine derivatives for next generation photosensitizer using photodynamic therapy of cancer, *Dyes and Pigments* 64 (1) (2005) 63–71.
- [44] Y. Liu, Y.S. Fan, Z.M. Liu, Pyrolysis of iron phthalocyanine on activated carbon as highly efficient non-noble metal oxygen reduction catalyst in microbial fuel cells, *Chemical Engineering Journal* 361 (2019) 416–427.
- [45] W.M. Ghasemi, R.W. Daud, M. Rahimnejad, M. Rezayi, A. Fatemi, Y. Jafari, M.R. Somalu, A. Manzour, Copper-phthalocyanine and nickel nanoparticles as novel cathode catalysts in microbial fuel cells, *International Journal of Hydrogen Energy* 38 (22) (2013) 9533–9540.
- [46] B. Mecheri, V.C.A. Ficca, M.A.C. de Oliveira, A. D'Epifanio, E. Placidi, F. Arciprete, S. Licoccia, Facile synthesis of graphene-phthalocyanine composites as oxygen reduction electrocatalysts in microbial fuel cells, *Applied Catalysis B: Environmental* 237 (2018) 699–707.
- [47] K. Müller, M. Richter, D. Friedrich, I. Paloumpa, U.I. Kramm, D. Schmeißer, Spectroscopic characterization of Cobalt-Phthalocyanine electrocatalysts for fuel cell applications, *Solid State Ionics* 216 (2012) 78–82.
- [48] J. Maruyama, M. Yamamoto, T. Hasegawa, S. Iwasaki, A. Mineshige, Carbonaceous thin film coated on nanoparticle as fuel cell catalyst formed by one-pot hybrid physical-chemical vapor deposition of iron phthalocyanine, *Electrochimica Acta* 90 (2013) 366–374.
- [49] S. Arucu, M.B. Sağılam, A.R. Özkaya, Electrochemical, spectroelectrochemical and electrocatalytic properties of newly synthesized phthalocyanine compounds with 1,1'-thiobis(2-naphthol) groups, *Journal of Molecular Structure* 1198 (2019) 126883.
- [50] E. Mshoperi, R. Fogel, J. Limson, Application of carbon black and iron phthalocyanine composites in bioelectricity production at a brewery wastewater fed microbial fuel cell, *Electrochimica Acta* 128 (2014) 311–317.
- [51] J. Champavert, S.B. Rejeb, C. Innocent, M. Pontié, Microbial fuel cell based on Ni-tetra sulfonated phthalocyanine cathode and graphene modified bioanode, *Journal of Electroanalytical Chemistry* 757 (2015) 270–276.
- [52] G. Lalande, G. Faubert, R. Côté, D. Guay, J.P. Dodelet, L.T. Weng, P. Bertrand, Catalytic activity and stability of heat-treated iron phthalocyanines for the electroreduction of oxygen in polymer electrolyte fuel cells, *Journal of Power Sources* 61 (1–2) (1996) 227–237.
- [53] M. Nemakal, S. Aralekallu, I. Mohammed, S. Swamy, L.K. Sannegowda, Electropolymerized octabenzimidazole phthalocyanine as an amperometric sensor for hydrazine, *Journal of Electroanalytical Chemistry* 839 (2019) 238–246.
- [54] E.T. Acar, T.A. Tabakoglu, D. Atilla, F. Yuksel, G. Atun, Synthesis, electrochemistry and electrocatalytic activity of cobalt phthalocyanine complexes – Effects of substituents for oxygen reduction reaction, *Polyhedron* 152 (2018) 114–124.
- [55] M. Shumba, T. Nyokong, Development of nanocomposites of phosphorus-nitrogen co-doped graphene oxide nanosheets and nanosized cobalt phthalocyanines for electrocatalysis, *Electrochimica Acta* 213 (2016) 529–539.
- [56] C. Barrera, I. Zhukov, E. Villagra, F. Bediou, M.A. Páez, J. Costamagna, J.H. Zagal, Trends in reactivity of unsubstituted and substituted cobalt-phthalocyanines for the electrocatalysis of glucose oxidation, *Journal of Electroanalytical Chemistry* 589 (2) (2006) 212–218.
- [57] K. Kantize, I.N. Booyesen, A. Mambanda, Electrochemical sensing of acetaminophen using nanocomposites comprised of cobalt phthalocyanines and multiwalled carbon nanotubes, *Journal of Electroanalytical Chemistry* 850 (2019) 113391.
- [58] M. Gulppi, S. Griveau, F. Bediou, J.H. Zagal, Electrocatalysis of 2-mercaptopropanesulfonic acid oxidation on cobalt phthalocyanine modified electrodes. Effect of surface concentration of the catalyst, *Electrochimica Acta* 46 (22) (2001) 3397–3404.
- [59] P.K. Sonkar, V. Ganesh, R. Gupta, D.K. Yadav, M. Yadav, Nickel phthalocyanine integrated graphene architecture as bifunctional electrocatalyst for CO₂ and O₂ reductions, *Journal of Electroanalytical Chemistry* 826 (2018) 1–9.
- [60] F. Harnisch, S. Wirth, U. Schröder, Effects of substrate and metabolite crossover on the cathodic oxygen reduction reaction in microbial fuel cells: Platinum vs. iron(II) phthalocyanine based electrodes, *Electrochemistry Communications* 11 (2009) 2253–2256.
- [61] S. Shahrokhan, M. Ghalkhani, M.K. Amini, Application of carbon-paste electrode modified with iron phthalocyanine for voltammetric determination of epinephrine in the presence of ascorbic acid and uric acid, *Sensors and Actuators B: Chemical* 137 (2) (2009) 669–675.
- [62] Z. Biyiklioglu, H. Baş, Synthesis and electrochemistry of non-aggregated axially disubstituted silicon phthalocyanines bearing benzoxazin substituents, *Inorganica Chimica Acta* 427 (2015) 293–298.
- [63] A. Günsel, A.T. Bilgiçli, E. Kirbaç, S. Güney, M. Kandaz, Water soluble quaternizable gallium and indium phthalocyanines bearing quinoline 5-sulfonic acid: Synthesis, aggregation, photophysical and electrochemical studies, *Journal of Photochemistry and Photobiology A: Chemistry* 310 (2015) 155–164.
- [64] K.-K. Türk, I. Kruusenberg, J. Mondal, P. Rauwel, J. Kozlova, L. Matisen, V. Sammelselg, K. Tammeveski, Oxygen electroreduction on Mn4-macrocycle modified graphene/multi-walled carbon nanotube composites, *Journal of Electroanalytical Chemistry* 756 (2015) 69–76.
- [65] H. Kantekin, G. Sarkı, A. Koca, O. Bekircan, A. Aktaş, R.Z.U. Kobak, M.B. Sağılam, Synthesis, structural characterizations, and electrochemical and spectroelectrochemical properties of novel peripherally octa-substituted metallophthalocyanines, *Journal of Organometallic Chemistry* 789–790 (2015) 53–62.
- [66] J. Losada, I. del Peso, L. Beyer, Redox and electrocatalytic properties of electrodes modified by films of polypyrrole nickel(II) Schiff-base complexes, *Journal of Electroanalytical Chemistry* 447 (1–2) (1998) 147–154.
- [67] A.M. Sevim, S. Çakar, M. Özçar, A. Güllü, Electrochemical and photovoltaic properties of highly efficient solar cells with cobalt/zinc phthalocyanine sensitizers, *Solar Energy* 160 (2018) 18–24.
- [68] A.P. Yuen, S.M. Jovanovic, A.M. Hor, R.A. Klenkler, G.A. Devenyi, R.O. Loutfy, J.S. Preston, Photovoltaic properties of M-phthalocyanine/fullerene organic solar cells, *Solar Energy* 86 (6) (2012) 1683–1688.
- [69] R. Signerski, B. Kościelska, Photovoltaic properties of a sandwich cell consisting of bromophosphorus phthalocyanine and titanium dioxide layers, *Optical Materials* 27 (9) (2005) 1480–1483.
- [70] M. Urbani, M.E. Ragoussi, M.K. Nazeeruddin, T. Torres, Phthalocyanines for dye-sensitized solar cells, *Coordination Chemistry Reviews* 381 (2019) 1–64.
- [71] R.S. Okazaki, M. Takeuchi, Effects of NO₂ on photovoltaic performance of phthalocyanine thin film solar cells, *Thin Solid Films* 334 (1–2) (1998) 187–191.
- [72] T.D. Anthopoulos, T.S. Shafai, Influence of oxygen doping on the electrical and photovoltaic properties of Schottky type solar cells based on α -nickel phthalocyanine, *Thin Solid Films* 441 (1–2) (2003) 207–213.
- [73] M. Soylu, R. Ocaya, H. Tuncer, A.A. Al-Ghamdi, A. Dere, D.C. Sarı, F. Yakuphanoglu, Analysis of photovoltaic behavior of Si-based junctions containing novel graphene oxide/nickel(II) phthalocyanine composite films, *Microelectronic Engineering* 154 (2016) 53–61.
- [74] E.N. Ovchenkova, N.G. Bichan, A.A. Ksenofontov, T.N. Lomova, New dyads based on trifluoromethylated phthalocyanine derivatives and substituted fullerene with possible application photoinduced electron transfer, *Journal of Fluorine Chemistry* 224 (2019) 113–120.
- [75] Q.D. Dao, A. Fujii, R. Tsuji, Y. Takeoka, M. Ozaki, Efficiency enhancement in perovskite solar cell utilizing solution-processable phthalocyanine hole transport layer with thermal annealing, *Organic Electronics* 43 (2017) 156–161.
- [76] G.Ö. Artuç, A. Altindal, B.B. Eran, M. Bulut, Synthesis, characterization and ethanol sensing properties of peripheral and non-peripheral tetrakis-(3,6-diethyl-7-oxy-4-methylcoumarin)substituted zinc(II), cobalt(II), and copper(II) phthalocyanines, *Dyes and Pigments* 171 (2019) 107741.
- [77] H.S. Soliman, A.A.M. Farag, N.M. Khosifan, M.M. El-Nahass, Electrical transport mechanisms and photovoltaic characterization of cobalt phthalocyanine on silicon heterojunctions, *Thin Solid Films* 516 (23) (2008) 8678–8683.
- [78] M. Ari, Z. Kanat, H. Dinger, Design, computational screening and synthesis of novel non-peripherally tetra hexylthio-substituted phthalocyanines as bulk heterojunction solar cell materials, *Solar Energy* 134 (2016) 1–8.
- [79] S. Gorduk, A. Altindal, Peripherally tetra-substituted metallophthalocyanines bearing carboxylic acid groups for efficient dye sensitized solar cells, *Journal of Molecular Structure* 1196 (2019) 747–753.
- [80] M.A. Ruderer, M. Hinterstocker, P. Müller-Buschbaum, Structure in ternary blend systems for organic photovoltaics, *Synthetic Metals* 161 (2011) 17–18 2001–2005.
- [81] H. Karaca, İ. Şişman, E. Güzel, S. Sezer, F. Selimoğlu, B. Ergezen, M. Karaca, V. Eyüpoglu, Thiochalcone substituted phthalocyanines for dye-sensitized solar cells: Relation of optical and electrochemical properties for cell performance, *Journal of Coordination Chemistry* 71 (2018) 1606–1622.
- [82] A.T. Gökçeören, E. Kaplan, Y. Arslanoğlu, Electrochemical and morphological analysis on novel phthalocyanine grafted conductive polymeric nanofibers, *Journal of Electroanalytical Chemistry* 729 (2014) 87–94.
- [83] F.G. Zamani, H. Moulahoum, M. Ak, D.O. Demirkol, S. Timur, Current trends in the development of conducting polymers-based biosensors, *TrAC Trends in Analytical Chemistry* 118 (2019) 264–276.
- [84] P. Eskandari, Z.A. Rezvani, H.R. Mamaqani, M.S. Kalajahi, H. Mardani, Polymer grafting on graphene layers by controlled radical polymerization, *Advances in Colloid and Interface Science* 273 (2019) 102021.
- [85] C. Coutanceau, A. El Houch, P. Crouigneau, J.M. Leger, C. Lamy, Conducting polymer electrodes modified by metal tetralsulfonated phthalocyanines: Preparation and electrocatalytic behaviour towards dioxygen reduction in acid medium, *Electrochimica Acta* 40 (17) (1995) 2739–2748.
- [86] S.A. Umoren, M.M. Solomon, Protective polymeric films for industrial substrates: A critical review on past and recent applications with conducting polymers and polymer composites/nanocomposites, *Progress in Materials Science* 104 (2019) 380–450.
- [87] A. Sanmatías, D. Benito, J. Navarro-Laboulais, J.J. Garcíá-Jareño, F. Vicente, Surface modification of graphite+polymer composite and ITO electrodes by Nafion®+cupromeric phthalocyanine films, *Electrochimica Acta* 45 (4–5) (1999) 797–808.
- [88] A.R. Karimi, F. Bayat, Synthesis of new highly organosoluble metallophthalocyanines with 1,8-dioxo-octahydroxanthene substituents, *Tetrahedron Letters* 53 (2) (2012) 123–126.
- [89] A. Filippova, A. Vashurin, S. Znayko, I. Kuzmin, M. Razumov, A. Chernova, G. Shaposhnikov, O. Koifman, Novel Co(II) phthalocyanines of extended periphery and their water-soluble derivatives. Synthesis, spectral properties and catalytic activity, *Journal of Molecular Structure* 1149 (2017) 17–26.

- [90] M.S. Ağırtaş, C. Karataş, S. Özdemir, Synthesis of some metallophthalocyanines with dimethyl 5-(phenoxy)-isophthalate substituents and evaluation of their antioxidant-antibacterial activities, *Spectrochimica Acta Part A: Molecular and Biomolecular Spectroscopy* 135 (2015) 20–24.
- [91] K. Bozorov, J. Zhao, H.A. Aisa, 1,2,3-Triazole-containing hybrids as leads in medicinal chemistry: A recent overview, *Bioorganic & Medicinal Chemistry* 27 (16) (2019) 3511–353.
- [92] M. Ansari, M. Shokrzadeh, S. Karima, S. Rajaei, S. Emami, Design, synthesis and biological evaluation of flexible and rigid analogs of 4H-1,2,4-triazoles bearing 3,4,5-trimethoxyphenyl moiety as new antiproliferative agents, *Bioorganic Chemistry* 93 (2019) 103300.
- [93] N.J.P. Subhashini, E.P. Kumar, N. Gurrapu, V. Yerragunta, Design and synthesis of imidazolo-1, 2,3-triazoles hybrid compounds by microwave-assisted method: Evaluation as an antioxidant and antimicrobial agents and molecular docking studies, *Journal of Molecular Structure* 1180 (2019) 618–628.
- [94] Y. Mahmoudi, H. Badali, S.M. Hashemi, M. Ansari, H. Fakhim, M. Fallah, M. Shokrzadeh, S. Emami, New potent antifungal triazole alcohols containing N-benzylpiperazine carbodithioate moiety: Synthesis, in vitro evaluation and in silico study, *Bioorganic Chemistry* 90 (2019) 103060.
- [95] N. Süleymanoğlu, R. Ustabas, Ş. Direkeli, Y.B. Alpaslan, Y. Ünver, 1,2,4-triazole derivative with Schiff base; thiol-thione tautomerism, DFT study and antileishmanial activity, *Journal of Molecular Structure* 1150 (2017) 82–87.
- [96] D.M. Mazur, M.E. Zimens, V.A. Bakulev, A.T. Lebedev, Identification and interconversion of isomeric 4,5-functionalized 1,2,3-thiadiazoles and 1,2,3-triazoles in conditions of electrospray ionization, *Journal of Pharmaceutical and Biomedical Analysis* 145 (2017) 315–321.
- [97] N. Süleymanoğlu, Y. Ünver, R. Ustabas, Ş. Direkeli, G. Alpaslan, Antileishmanial activity study and theoretical calculations for 4-amino-1,2,4-triazole derivatives, *Journal of Molecular Structure* 1144 (2017) 80–86.
- [98] Ö. Koyun, S. Gördük, B. Keskin, A. Çetinkaya, A. Koca, U. Avciata, Microwave-assisted synthesis, electrochemistry and spectroelectrochemistry of phthalocyanines bearing tetra terminal-alkynyl functionalities and click approach, *Polyhedron* 113 (2016) 35–49.
- [99] H. Karaca, S. Sezer, Ş. Özalp-Yaman, C. Tanyeli, Concise synthesis, electrochemistry and spectroelectrochemistry of phthalocyanines having triazole functionality, *Polyhedron* 72 (2014) 147–156.
- [100] M. Hasan, M. Shalaby, Synthesis, click reaction, molecular structure, spectroscopic and DFT computational studies on 3-(2,6-bis(trifluoromethyl)phenoxy)-6-(prop-2-yn-1-yloxy)phthalonitrile, *Journal of Molecular Structure* 1113 (2016) 88–98.
- [101] Ü. Demirbaş, D. Akyüz, H.T. Akçay, A. Koca, H. Kantekin, Non-peripherally tetra substituted lead(II), nickel(II) and copper(II) phthalocyanines bearing [1,2,3] triazole moieties: Synthesis, characterization and investigation of electrochemical and spectroelectrochemical properties, *Journal of Molecular Structure* 1176 (2019) 695–702.
- [102] H. Shinohara, O. Tsaryova, G. Schnurpeil, D. Wöhrl, Differently substituted phthalocyanines: Comparison of calculated energy levels, singlet oxygen quantum yields, photo-oxidative stabilities, photocatalytic and catalytic activities, *Journal of Photochemistry and Photobiology A: Chemistry* 184 (2006) 50–57.
- [103] Y. Pana, W. Chenb, S. Lub, Y. Zhang, Novel aqueous soluble cobalt phthalocyanine: synthesis and catalytic activity on oxidation of 2-mercaptoethanol *Dyes and Pigments*, 66, 2, 2005, 115–121.
- [104] V.I. Iliev, A.I. Ileva, L.D. Dimitrov, Catalytic oxidation of 2-mercaptoethanol by cobalt(II)-phthalocyanine complexes intercalated in layered double hydroxides, *Applied Catalysis A: General* 126 (2) (1995) 333–340.
- [105] H. Karaca, N. Akçay, M. Teker, Porphyrazine immobilization on polyester fabric and heterogeneous catalytic application on oxidation of 2-mercaptoethanol, *Fresenius Environmental Bulletin* 25 (5) (2016) 1714–1718.
- [106] A.L. Spek, Single-crystal structure validation with the program PLATON, *Journal of Applied Crystallography* 36 (2003) 7–13.
- [107] A.L. Spek, Structure validation in chemical crystallography, *Acta Crystallographica Section D* D65 (2009) 148–155.
- [108] APEX2, Version 2014.9-0, Bruker AXS Inc., Madison, WI, 2014.
- [109] SAINT, Version 8.34ABruker, Bruker AXS Inc., Madison, WI, 2013.
- [110] SADABS, Version2014/4Bruker, Bruker AXS Inc., Madison, WI, 2014.
- [111] G.M. Sheldrick, Crystal structure refinement with SHELXL, *Acta Crystallographica Section C* C71 (2015) 3–8.
- [112] O.V. Dolomanov, L.J. Bourhis, R.J. Gildea, J.A.K. Howard, H. Puschmann, OLEX2: a complete structure solution, refinement and analysis program, *Journal of applied crystallography* 42 (2009) 339–341.
- [113] M.J. Frisch, G.W. Trucks, H.B. Schlegel, G.E. Scuseria, M.A. Robb, J.R. Cheeseman, G. Scalmani, V. Barone, G.A. Petersson, H. Nakatsuji, X. Li, M. Caricato, A.V. Marenich, J. Bloino, B.G. Janesko, R. Gomperts, B. Mennucci, H.P. Hratchian, J.V. Ortiz, A.F. Izmaylov, J.L. Sonnenberg, D. Williams-Young, F. Ding, F. Lipparini, F. Egidi, J. Goings, B. Peng, A. Petrone, T. Henderson, D. Ranasinghe, V.G. Zakrzewski, J. Gao, N. Rega, G. Zheng, W. Liang, M. Hada, M. Ehara, K. Toyota, R. Fukuda, J. Hasegawa, M. Ishida, T. Nakajima, Y. Honda, O. Kitao, H. Nakai, T. Vreven, K. Throssell, J.A. Montgomery Jr., J.E. Peralta, F. Ogliaro, M.J. Bearpark, J.J. Heyd, E.N. Brothers, K.N. Kudin, V.N. Staroverov, T.A. Keith, R. Kobayashi, J. Normand, K. Raghavachari, A.P. Rendell, J.C. Burant, S.S. Iyengar, J. Tomasi, M. Cossi, J.M. Millam, M. Klene, C. Adamo, R. Cammi, J.W. Ochterski, R.L. Martin, K. Morokuma, O. Farkas, J.B. Foresman, D.J. Fox, Gaussian 16, Revision C.01, Gaussian, Inc., Wallingford CT, 2016.
- [114] R. Dennington, T.A. Keith, J.M. Millam, GaussView, Version 6, Semichem Inc., Shawnee Mission, KS, 2016.
- [115] C. Lee, W. Yang, R.G. Parr, Development of the Colle-Salvetti correlation-energy formula into a functional of the electron density, *Phys. Rev. B* 37 (1988) 785–789.
- [116] M.P. Cormick, M. Rovera, E.N. Duranini, Synthesis, spectroscopic properties and photodynamic activity of a novel Zn(II) phthalocyanine substituted by flucnizole groups, *Journal of Photochemistry and Photobiology A: Chemistry* 194 (2–3) (2008) 220–229.
- [117] M.J. Turner, J.J. McKinnon, S.K. Wolff, D.J. Grimwood, P.R. Spackman, D. Jayatilaka, M.A. Spackman, CrystalExplorer17, University of Western Australia, 2017 <http://hirshfeldsurface.net>.
- [118] A. Günsel, A.T. Bilgiçli, H. Pişkin, B. Tüzün, N. Ç. Delibaş, M. N. Yarasir, B. Gündüz, Comparison of spectroscopic, electronic, theoretical, optical and surface morphological properties of functional manganese(III) phthalocyanine compounds for various conditions, *Journal of Molecular Structure* 1193 (2019) 247–264.
- [119] Y. Pan, W. Chen, S. Lu, Y. Zhang, Novel aqueous soluble cobalt phthalocyanine: synthesis and catalytic activity on oxidation of 2-mercaptoethanol, *Dyes and Pigments* 66 (2005) 115–121.